III International Symposium

TOPICAL PROBLEMS OF BIOPHOTONICS

ADVANCED LASERS IN BIOMEDICINE

Chairs

Patrick Audebert, Ecole ***Polytechnique,*** Palaiseau, ***France***

Vladislav Panchenko, Institute on Laser and Information Technologies RAS, Moscow, Russia

Herbert Stepp, ***Laser Research*** laboratory, LIFE Center, ***University Clinic, Munich, Germany***

Program Committee

Victor Bagratashvili, Institute of Laser and Information Technologies RAS, Russia

Michael Bakunov, University of Nizhny Novgorod, Russia

Boris Chichkov, Laser Zentrum Hannover e.V., Germany

Felix Feldchtein, Dental Photonics Inc., USA; Institute of Applied Physics RAS, Russia

Efim Khazanov, Institute of Applied Physics RAS, Russia

Yury Malakhov, International Science and Technology Center, Russia

Alexander Sergeev, Institute of Applied Physics RAS, Russia

CUTTING EFFECTS INDUCED BY 2-μm LASER RADIATION OF CW Tm:YLF AND CW AND Q-SWITCHED Ho:YAG LASERS ON *EX-VIVO* TISSUE

O.L. Antipov[1], N.G. Zakharov[1], M. Fedorov[2], N.M. Shakhova[1,3], N.N. Prodanets[3], L.B. Snopova[3], V.V. Sharkov[1,4], and **R. Sroka[2]**

[1] Institute of Applied Physics RAS, Nizhny Novgorod, Russia, antipov@appl.sci-nnov.ru
[2] Laser-Research Laboratory, LIFE Center, Ludwig Maximilians University, Munich, Germany
[3] Nizhny Novgorod Medical Academy, Russia
[4] Nizhny Novgorod State University, Russia

Laser radiation in the 2-μm wavelength region is well-absorbed by water and has good transmittance through commercially available, low-OH quartz optical fibers which are generally acknowledged to have great potential for medical applications in endoscopic and open surgery [1]. Medical laser systems in this wavelength range are flash-lamp or laser-pumped pulsed Ho:YAG lasers and continuous wave (cw) thulium (Tm)-doped fiber or Tm:YAG lasers. This paper presents the laser–tissue effects on an *ex-vivo* tissue model using an innovative diode-pumped cw Tm:YLF laser and cw and Q-switched Ho:YAG laser [2, 3].

Innovative Tm:YLF and Ho:YAG lasers

The diode-pumped air-cooled Tm:YLF laser (IAP RAS prototype [2]) consists of a Tm:YLF rod, longitudinally and simultaneously pumped from the opposite ends by two fiber-coupled diode laser bars at $\lambda = 792$ nm (Coherent GmbH, Germany; optical output power up to 45 W). The laser elements and the cavity were optimized to obtain the maximum output power and high conversion efficiency. As a result of the optimization process, a laser emitting light was created in the cw mode at $\lambda = 1909$ nm with a maximum output power of 31 W. The slope efficiency for the output power was > 50% and the optical efficiency was 47%. Small divergence of the laser radiation (M^2-parameter was less than 1.3) offers a good opportunity for efficient coupling of the laser light into optical fibers.

The Ho:YAG laser (IAP RAS prototype [3]) is pumped by the radiation of a Tm:YLF laser. The active rod of the Ho:YAG laser was 25 mm in length with an undoped diffusion bonded end-cap. The laser cavity was formed by a flat mirror with high reflectivity, a flat 45° dichroic mirror with high reflectivity at the wavelength of $\lambda = 2090$ nm and a high transmission at the pump wavelength of $\lambda = 1909$ nm, together with a concave output coupler. To obtain maximum output power, the pump beam diameter inside the active element was expanded within the range of 0.53–0.8 mm; the output-coupler curvature varied from 150 to 300 mm. The physical resonator length varied during the optimization process from 5 to 25 cm. The Ho:YAG laser emitted light at the wavelength of $\lambda = 2090$ nm with the average laser power of up to 10W in the cw and Q-switched mode. The optical-to-optical efficiency reached values of > 55%. The introduction of a silica acousto-optic modulator (AOM) in front of the output coupler changed the cw system into a pulsed Q-switched laser emitting laser pulses of pulse durations of 25–100 ns at tunable repetition rates between 3 and 15 kHz resulting in peak powers of 125 kW and 25 kW, respectively. The laser beam quality of the Ho:YAG laser is about $M^2 < 1.2$ and can be easily coupled in low-OH optical fibers with core diameter of 300–600 μm.

***Ex-vivo* experiments**

Laser–tissue interaction experiments were performed using porcine kidney and liver tissue. For the experiments the laser radiation was transferred from the laser to the tissue via a low-OH flat-cut bare-ended optical fiber with a core diameter of 600 μm. The fiber end was positioned perpendicular to the tissue surface, either in non-contact (single-spot experiments) or in contact (cutting experiments) according to different potential clinical approaches.

Single-spot and cutting experiments were performed in a reproducible set-up. In the single-spot experiments, a fixed distance was used between fiber and tissue surface of $d = 5$ mm and energies were applied in the 10–200 J range. The cutting experiments were performed with the same laser parameters but in contact mode ($d = 0$ mm) using a constant scanning velocity of $v = 1$ mm/s of the linear fiber movement. Macroscopic and histological evaluations were performed.

Results and Discussion

Immediate tissue effects could be observed showing superficial coagulation, carbonization, vaporization and ablation [4]. The ablation depth differed with respect to the tissue, laser operation regime and with increasing applied energy (Fig. 1).

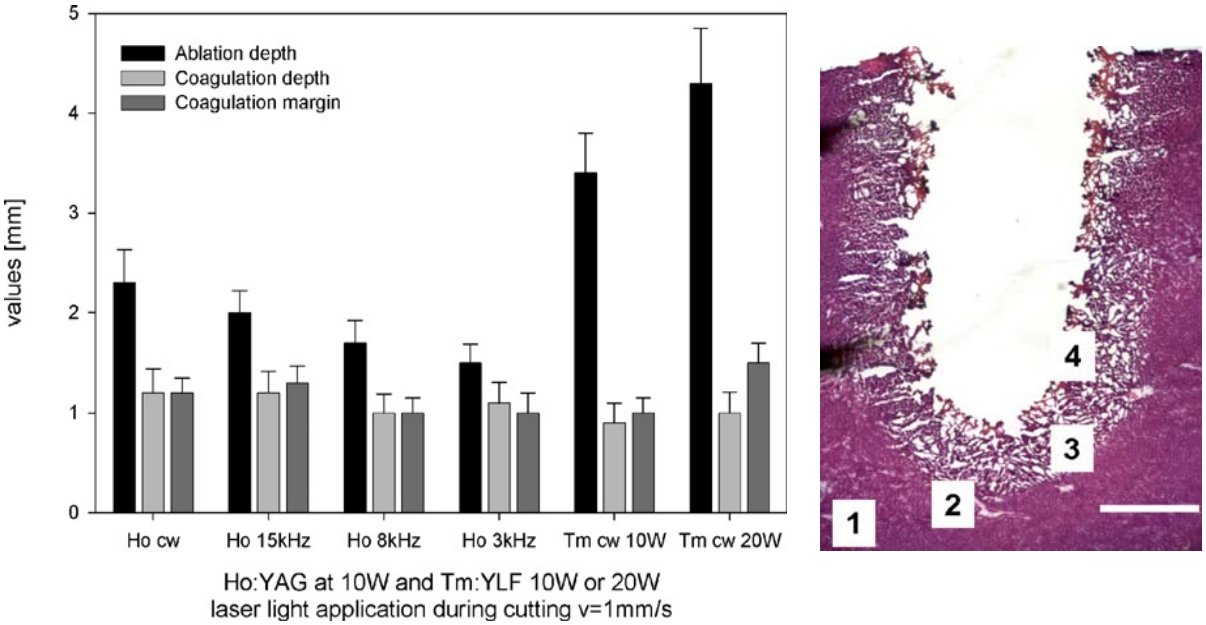

Fig. 1. Cutting experiments (fiber–tissue distance d = 0 mm, scanning velocity v = 1 mm/s) on porcine kidney tissue using Ho:YAG laser either in cw or in Q-switched mode at repetition rates of 15, 8 and 3 kHz (P=10W, t = 10 s) resulting in total applied energy of 100 J and Tm:YLF laser in cw mode at output power of 10 W and 20 W resulting in total applied energy of 100 and 200 J, respectively. Mean and standard deviations of ablation depth, axial coagulation depth and width of the radial coagulation rim are shown. The normal unaffected tissue "1", "2" heat-affected tissue, "3" coagulated tissue showing vacuolization, and "4" signs of carbonized tissue are shown on the right insert (bar: 1 mm)

As these effects in cutting or single-spot application depend on the specific optical and thermal tissue parameters, it is of interest that especially the coagulation in axial and radial direction showed comparable sizes without any significant differences. Thus the affected remaining tissue showed the same degree of thermal damage in both the lateral and the axial planes (the thickness of the coagulation zone in lateral and axial plane was nearly constant at 1±0.5mm in each direction).

Conclusion

The presented lasers showed good flexibility in the use for surgical approaches. The induced tissue effects showed a very high reproducibility in ablation and in coagulation for both radial and axial planes. The fact that the ablation thermal effects on the remaining tissue are limited to 1 ± 0.5 mm is encouraging with regard to the potential for the laser-assisted preparation near to sensitive structures. The sealing capacity of the system as well as its potential for its use in the thermal occlusion of vessels must be investigated in perfused tissue models.

References

1. K. Scholle, et al., 2 μ*m laser sources and their possible applications*. In: P. Bishnu, editor. Frontiers in guided wave optics and optoelectronics. Vucovar: INTECH Publishing; 2010. p. 471-500.
2. N.G. Zakharov, et al., *Quantum Electron.,* 2009, **39**(5), 410-417.
3. N.G. Zakharov, et al., *Quantum Electron.,* 2010, **40**(2), 98-100.
4. O.L. Antipov, et al., *Med. Laser Applications,* 2011.

Invited

LASER-INDUCED HYDRODYNAMICS NEARBY OPTICAL FIBER TIP

V.N. Bagratashvili[1], **V.I. Yusupov**[1,2], and **V.M. Chudnovskii**[2]

[1] Institute on Laser and Information Technologies, Russian Academy of Sciences
Pionerskaya ul. 2, Troitsk, Moscow Region, Russia, bagrat@laser.ru
[2] Il'ichev Pacific Institute of Oceanology, Far East Division, Russian Academy of Sciences
Baltiiskaya ul. 43, Vladivostok, Russia

These studies are aimed at revealing the mechanisms of therapeutic effects stimulated by medium power (1–10 W) fiber laser induced hydrodynamics in water-saturated bio-tissues. Modern laser medical technologies widely employ delivery of laser radiation to the irradiated tissues via optical fibers. Optical fibers easily penetrate through needles and endoscopic channels, and lasers can be used for puncture and endoscopic operations. Several laser medical technologies (fractional photo-thermolysis, laser engineering of cartilages, puncture multichannel laser decompression of disc, laser intervention upon osteochondrosis, surgical treatment of chronic osteomyelitis, endovenous laser ablationб etc.) are based on the effective hydrodynamic processes in water-saturated bio-tissues. These hydrodynamic processes trigger cellular response and regenerative effects through the mechanisms of mechano-biology. We study hydrodynamic effects induced by the moderate power laser radiation in the vicinity of the heated end surface of optical fiber in water, in particular, the generation of air–vapor bubbles, effects of laser-induced filaments formation and degradation of transport optical fiber.

Generation of Bubbles in Liquid. The effective hydrodynamic processes in water are related to the explosive boiling in the vicinity of the heated end surface of the fiber. The resulting bubbles with sizes ranging from several to several tens of microns have velocities of up to 100 mm/s in the vicinity of the end surface. The generation of bubbles in a capillary gives rise to the stable circulation of liquid with the period ranging from 0.2 to 1 s. At a laser power of less than 3 W, stable bubble microjets, which consist of the bubbles whose sizes range from several to ten microns, can be generated in the vicinity of the blackened end surface.

Degradation of optical fiber tip. We have studied the process of degradation of optical fiber tip as a result of hydrodynamic processes caused by medium power (1–5 W) cw laser effects on connective tissues. The temperature nearby optical fiber tip can be as high as several thousands of degrees. It is shown, that such high values of temperature and pressure caused by cavitation collapse of microbubbles result in formation of nano-size diamonds on the tip and, also, in water transition to supercritical state, that promotes degradation of optical fiber tip.

Formation of filaments. Medium power (0.3–8.0 W) 970 nm in wavelength laser irradiation of water with added Ag nanoparticles (in the form of Ag-albumin complexes) through 400 μm optical fiber stimulates self-organization of filaments of Ag nanoparticles for a few minutes. These filaments represent themselves long (up to 14 cm) liquid gradient fibers with unexpectedly thin (10–80 ¹m) core diameter. They are stable in the course of laser irradiation being destroyed after laser radiation off. Such effect of filaments of Ag nanoparticles self-organization is rationalized by the peculiarities of laser-induced hydrodynamic processes developed in water in presence of laser light and by formation of liquid fibers.

STUDY OF PHOTOSENSITIZERS UPTAKE AND INTRACELLULAR DISTRIBUTION IN HUMAN NORMAL AND MALIGNANT CELL LINES

A.A. Brilkina[1], **L.V. Dubasova**[1], **I.V. Balalaeva**[1,2], **E.A. Sergeeva**[2], **A.R. Katichev**[1], and **N.M. Shakhova**[2]

[1] N.I. Lobachevsky State University of Nizhni Novgorod, Nizhny Novgorod, Russia, annbril@mail.ru
[2] Institute of Applied Physics, RAS, Nizhny Novgorod, Russia

The fundamental concept of photodynamic therapy (PDT) is predominant accumulation of photosensitizers (PSs) in cancer cells compared to healthy cells which allows minimizing negative impact during tumor treatment [1]. Therefore, the study of uptake dynamics and subcellular localization of newly developed PDT agents in both normal and tumor cells, as well as their cytotoxicity, is of high importance. PSs can be accumulated either in cellular membrane and lysosomes leading to cell necrosis as the result of treatment, or in mitochondria, Golgi apparatus and endoplasmic reticulum causing apoptosis, the most desired PDT outcome [2, 3]. The goal of the proposed work is comparative analysis of uptake dynamics and subcellular distribution of different types of photosensitizers in normal and malignant cells lines.

We studied PDT agents produced by Russian pharmaceutical companies: Alasens (5-ala) based on Aminolevulinic acid, chlorine derivative Photoditasin (PhD) and phthalocyanine derivatives Photosens (PhoS), Ftalosens (FtS) and Holosens (HoS). The properties of all PSs were tested with cell lines of normal hepatocytes (Chang Liver) and human hepatocellular carcinoma (SK-HEP-1). Cells were grown in culture medium EMEM with glutamine, 10% fetal bovine serum and incubated at 37°C with 5% CO_2. For the study of PSs uptake the cells were incubated with the up mentioned solutions of the following concentrations: PhoS, FtS and HoS, 10 μg/ml in the growth media; PhD, 40 μg/ml; 5-ala, 0,8 mg/ml. Dynamics of PSs accumulation was estimated by flow cytometry method (FACSCalibur, BD, USA). For this study cells were incubated in a 24-well plate with a PS for the time of 5 min up to 24 hours, then removed from the plate, and the level of intracellular fluorescence under laser excitation at 633 nm was analyzed. Intracellular localization of PSs was monitored using Axiovert 200M LSM 510 META laser scanning microscope (Carl Zeiss GmbH, Germany). For LSM study the cells were seeded to the glass-bottom Petri dishes. Incubation time varied depending on the PS type: 2 hours for all exogenous PSs, and 3 hours for 5-ala which is the precursor of endogenous protoporphyrin IX (PpIX). In order to investigate PSs intracellular distribution the organelles (mitochondria, lysosomes, Golgi apparatus and endoplasmic reticulum) were stained by MitoTracker green, LysoTracker green, NBD- and BODIPY Dye-Labeled Sphingolipids and ER-Tracker green. All the dyes and drugs were washed out before LSM observation. All PSs were excited at 633 nm, fluorescence was detected at 650-710 nm; fluorescence of stained organelles was excited at 488 nm and registered in the range 500-530 nm.

Flow cytometry experiments revealed that in the presence of 5-ala the maximum of PpIX accumulation in normal cell lines was observed in 3 hours versus 6 hours for malignant cell lines. PpIX content in malignant cells at maximum accumulation time was twice as high compared to normal cells. Both normal and malignant cell lines demonstrated slow decrease of PpIX fluorescence after reaching maximum. For all exogenous PSs we observed increasing uptake during 4-8 hours followed by saturation of accumulation without significant signal decrease. Accumulation of PhD in malignant cells was 15-20% higher related to normal cells. For PhoS, FtS and HoS we detected no difference in their accumulation in malignant cells compared to normal cells.

LSM study of intracellular distribution of most PDT agents demonstrated no principal difference in photosensitizer localization in normal versus malignant cells. PpIX allocation in cancer cells was almost homogeneous with increased density in perinuclear region (Fig. 1). At the same time, PpIX distribution in normal cells was more homogeneous.

Exogenous PhD and FtS were observed in membrane structures of both normal and cancer cells (Fig. 2). On the basis of colocalization analysis of PSs and organelles fluorescence we concluded that these photosensitizers are accumulated in Golgi apparatus. Phthalocyanine derivatives PhoS and HoS were accumulated in vesicles some of which were distinguished as lysosomes (Fig. 3).

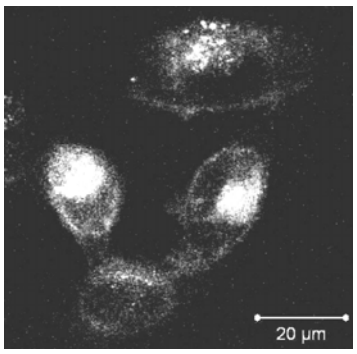

Fig. 1. Intracellular distribution of 5-ala induced PpIX in SK-HEP-1 cells.
Objective 63x/1.4; bar 20 µm; PpIX ex/em = 633/650-710 nm

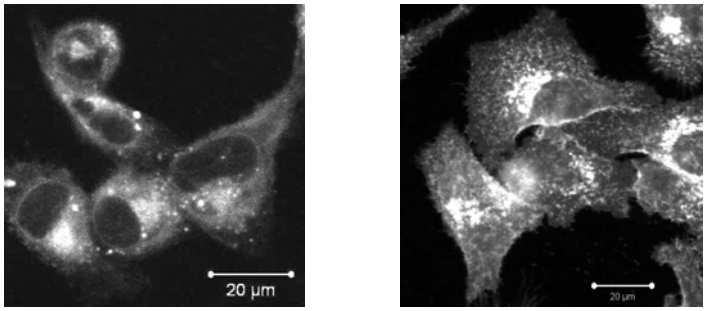

Fig. 2. Intracellular distribution of Photoditasin in SK-HEP-1 cells (left) and Ftalosens in Chang liver cells (right). Objective 63x/1.4; ex/em = 633/650-710 nm

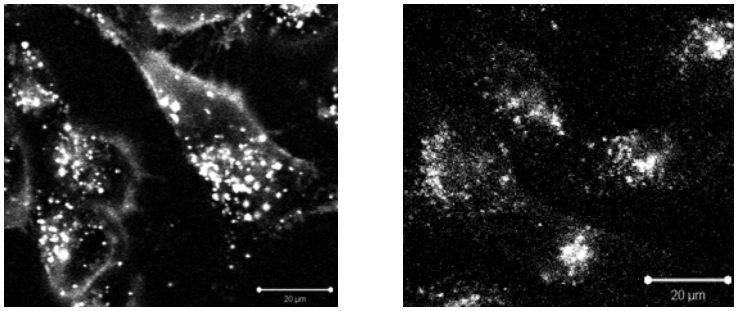

Fig. 3. Intracellular distribution of Photosens in SK-HEP-1 cells (left) and Holosens in Chang liver cells (right). Objective 63x/1.4; ex/em = 633/650-710 nm

As a summary, we found that endogenous photosensitizer PpIX is accumulated in malignant cells and retains there with higher efficiency compared to normal cells. Exogenous Photoditasin also demonstrates better uptake in cancer related to normal cells, with typical localization in cell membrane for both types of cells. Similar membrane distribution is observed for Ftalosens, whereas other two Phthalocyanine derivatives Photosens and Holosens are accumulated in vesicles in both normal and malignant cells. All Phthalocyanine derivatives demonstrate similar uptake dynamics.

Acknowledgements

This work was partially supported by the Russian Foundation for Basic Research (11-02-00916-a) and the Program of RAS Presidium "Fundamental Sciences for Medicine".

References

1. D. Dolmans, D. Fukumura and RK. Jain, *Nature Reviews Cancer,* 2003, **3**(5), 380-387.
2. G. Begum, A. Dube, P.G. Joshi, P.K. Gupta and N.B. Joshi, *J. Photochem. Photobiol., B: Biol*., 2009, **95**(3), 177-184.
3. J. Saczko, M. Mazurkiewicz, A. Chwiłkowska, J. Kulbacka, G. Kramer, M. Ługowskim, M. Śnieturam, T. Bana, *Folia Biologica*., 2007, **53**, 7-12.

TEMPERATURE CONTROLLED RETINAL PHOTOCOAGULATION

R. Brinkmann[1,3], S. Koinzer[2], K. Schlott[1,3], L. Ptaszynski[2], M. Bever[2], A. Baade[1], Y. Miura[3], J. Roider[3], and **R. Birngruber[1,3]**

[1] Medical Laser Center Lübeck, Lübeck, Germany
[2] Eye Clinic University of Schleswig-Holstein, Campus Kiel, Germany
[3] Institute of Biomedical Optics, University of Lübeck, Lübeck, Germany
e-mail: brinkmann@mll.uni-luebeck.de

Retinal photocoagulation is a long time established treatment for a variety of retinal diseases, most commonly applied for diabetic macular edema and diabetic retinopathy. The damage extent of the induced thermal coagulations depends on the temperature increase and the time of irradiation. So far, the induced temperature rise is unknown due to intraocular variations in light transmission as well as scattering and RPE/choroidal pigmentation, which can vary inter- and intraindividually by more than a factor of four. Thus, in clinical practice, often stronger and deeper coagulations are applied than therapeutically required, which lead to extended retinal damage and strong pain perception.

In this project, an optoacoustic (OA) method is developed to determine the temperature rise during retinal photocoagulation. The principle of OA and OA temperature determination relies on the short pulsed laser irradiation and heating of an absorber, which subsequently leads to thermoelastic expansion and the emission of bipolar pressure [1]. The amplitude of the pressure wave $p(t)$ is proportional to the pulse energy E_0 and the material specific Grüneisen parameter $\Gamma(T)$ according to $P(T) \sim \Gamma(T)E_0$. The temperature dependence of $\Gamma(T)$ can be approximated as a 2nd order polynomial in the range of 20–80°C

$$\Gamma(T) \sim \left((T^2 - T_0^2) - 2T_{\max}(T - T_0) \right)$$

T_0 represents the temperature, for which $\Gamma(T_0) = 0$ and T_{max} is the peak of the parabolic approximation. With the amplitude $p(t)$ of the detected pressure wave the tissue temperature can therefore be expressed as [2]:

$$T_{OA}(t) = T\left(p(t), t\right) = T_{\max} - \sqrt{\left(T_{\max} - T_0\right)^2 + \frac{p(t)}{S \cdot E_{abs}}} \qquad (1)$$

The factor S takes into account individual parameters, such as absorption and scattering as well as pressure propagation from the source to the detector and the transducer characteristics. In order to determine T_0 and T_{max}, the globes were fixed in a holder which allowed laser heating from rear with about 1°C/s [3], while measuring the pressure waves at the cornea with a modified contact lens containing an embedded acoustic transducer, and retinal temperatures with thermo-couples at the retina. A significant pressure rise of about 75% from 10 °C to 40 °C was found [3]. With a least square regression fit, T_0 and T_{max} were determined to be $T_0 = -17.0 \pm 5.0$°C and $T_{max} = 93.3 \pm 15.6$°C as average value with standard deviation of the parameters determined from 18 porcine eyes [3].

A clinical study comprising 20 patients is conducted in order to determine the temperature rise during photocoagulation. Irradiation is performed with defined laser settings in the arcades of the fundus and with routine parameters for coagulation on the treatment site. A modified photocoagulation laser (Zeiss Visulas 532 s, $\lambda = 532$ nm) was used for treatment. The treatment radiation is superimposed by ns probe laser pulses applied with a repetition rate of 1 kHz and adjustable probe pulse energies. The acoustic transients are measured with the modified contact lens. Prior to each exposure, calibration laser pulses are applied in order to determine S according to eq. 1 by making use of the fact that any pressure measured prior to laser treatment refers to body temperature.

Figure 1 shows a fundus picture of a patient post treatment and the central RPE temperature slopes for selected coagulation sites calculated by eq. 1, however, corrected for the beam profile and exponential absorption decay [3]. The clinical data evaluation shows very similar temperature profiles and absolute temperatures for most of the lesions ranging from 60–80°C. The observed temperature slopes are within the range which is expected from heat diffusion theory. However, when comparing the measured with the calculated temperature rise it turns out that just around 30% of the power which is emitted from the slit lamp seems to reach the retina, most likely owing to light scattering in the lens

and vitreous of the patients. Further it is interesting to note that the absolute temperatures determined are much smaller than predicted by the standard Arrhenius parameters for the threshold of coagulation, e.g. 75°C for 100 ms [4].

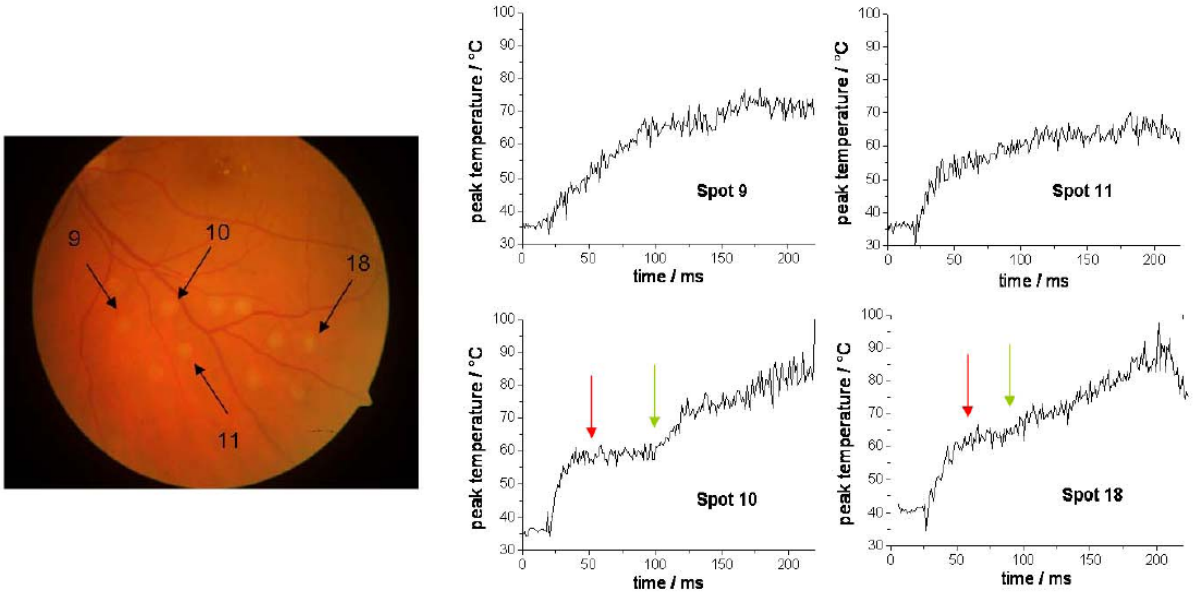

Fig. 1. Patients fundus picture post treatment and selected peak temperature curves.
Treatment: spot diameter 300 µm, laser power 200 mW, irradiation time 200 ms, probe pulse energy 12 µJ

In conclusion, it is shown that optoacoustics can serve to measure increasing pressure amplitudes during retinal photocoagulation, which can be used to calculate the temperature during the irradiation process. In this ongoing project it has already been demonstrated on enucleated porcine eyes and in vivo on rabbits that these data can be processed in real time and be used for an automatic treatment laser switch-off on preselected coagulation strengths, when the appropriate temperature is reached [5].

Acknowledgement

This collaborative project is supported by the German Ministry of Research and Technology (BMBF) under the Innovation Price for Advancing Medical Technology in 2006.

References

1. M.W. Sigrist and F.K. Kneubühl, "Laser-generated stress waves in liquids," *J. Acoust. Soc Am.,* 1978, **64**(6), 1652-1663.
2. J. Kandulla, H. Elsner, R. Birngruber, R. Brinkmann, "Noninvasive optoacoustic online retinal temperature determination during continuous-wave laser irradiation", *J. Biomed. Opt*., 2006, **11**(4), 041111.
3. R. Brinkmann, S. Koinzer, K. Schlott, L. Ptaszynski, M. Bever, A. Baade, S. Luft, Y. Miura, R. Birngruber, J. Roider, "Realtime Temperature Determination during Retinal Photocoagulation on Patients", *Proceeding SPIE*, 2011, **7885**.
4. R. Birngruber, F. Hillenkamp, V.P. Gabel, "Theoretical investigations of laser thermal retinal injury", *Health Phys*., 1985, **48**(6), 781-796.
5. K. Schlott, S. Koinzer, L. Ptaszynski., M. Bever, A. Baade, J. Roider, R. Birngruber, R. Brinkmann, "Optoacoustic Temperature Determination and Automatic Coagulation Control in Rabbits", *Proceeding SPIE*, 2011, 7885.

PLANING OF PDT OF CERVICAL NEOPLASIA WITH OPTICAL INTROSCOPY

D.D. Bundina[1], O.V. Kachalina[1], I.A. Kuznetsova[3], E.V. Grebenkina[4], and **N.M. Shakhova[2,1]**

[1] State Medical Academy, Nizhny Novgorod, Russia, dd-bundina@yandex.ru
[2] Institute of Applied Physics of the RAS, Nizhny Novgorod, Russia
[3] Regional Hospital, Nizhny Novgorod, Russia
[4] Regional Oncological Hospital, Nizhny Novgorod, Russia

Cervical cancer (CC) is actual medical and social problem. One of the directions for CC prevention is adequate treatment of cervical intraepithelial neoplasia (CIN) [1]. Due to modern tendencies towards "rejuvenation" of CC and CIN accurate timely diagnostics and organ-preserving methods of treatment are of importance [2]. PDT is a method of choice for treatment of CIN in females of reproductive age which is ensured by combination of efficiency and organ-preservation. Unfortunately, the method is not sufficiently introduced into clinical practice. One of the reasons is imperfection of diagnostic techniques. Thus, “the gold standard” CIN diagnostics are colposcopy (CS) and direct biopsy. However, recent studies have shown that colposcopic and histological criteria of neoplastic changes often do not correlate which decreases sensitivity of colposcopically guided biopsy. This fact is caused by subjectivism in evaluation of colposcopic criteria, *kappa* is only 0.17-0.26. For increase in accuracy of early cervical neoplasia diagnostics random biopsies or wide excisions are proposed [3, 4]. Alternative for this tactics is combined application of CS and novel noninvasive diagnostic techniques such as fluorescent diagnostics or high-resolution introscopy [5].

Materials and methods

In this work in addition to standard CS we employ optical coherence tomography (OCT). OCT is a novel high-resolution non-invasive technique for in vivo imaging of inner microstructure of biotissues with resolution at tissue layer level (15–20 μm). Earlier conducted studies demonstrates high diagnostic efficiency of OCT in case of cervix neoplasia: sensitivity is 82%, specificity is 78%, *kappa* is 0.65. In this work we used OCT in screening (cytology and HPV test) positive patients Criteria for inclusion are early neoplasia (dysplasia and cancer *in situ*) and reproductive age of patients.

Results and conclusion

As a result of the study we have developed a diagnostic protocol including following consequence of diagnostic procedures: colposcopy, OCT, biopsy. At the stage of primary diagnostics OCT makes it possible to avoid random biopsies. At the stage of diagnosis specification and treatment planning OCT data allows to validate the choice of treatment method and in particular cases to substitute broad excisions with PDT. At the stage of follow-up OCT allows for noninvasive evaluation of healing process. In long-term follow-up OCT data can be used for early recurrence diagnostics.

In our opinion, the developed diagnostic algorithm employing optical introscopy will allow to apply individual treatment tactics in young patients with cervix neoplasia, to expand indications for PDT and to provide noninvasive treatment monitoring which will finally promote efficient prevention of cervix cancer with preserving of reproductive function.

Acknowledgements

The authors thank the RFBR (08-02-99049-р_офи, 11-02-00916-а) and Presidium of RAS for the financial support of this work. The authors are also grateful to the staff and management of the Nizhny Novgorod Regional Hospital and Regional Oncological Hospital for the possibility to conduct this research study.

References

1. *NHO Weekly epidemiological record*, 2009, **15**, 116-132.
2. G. Ronco, P. Rossi, *Cancer Epidemiol Biomarkers Prev*., 2008, **17**, 3033-42.
3. L.S. Massad, Y.C. Collins, *Gynecol. Oncol*., 2003, **89**, 424-8.
4. J.C. Gage, V.W. Hanson, K. Abbey, et al., *Obstet Gynecol*., Aug, 2006, **108**(2), 264-272.
5. C.A. Balas, *IEEE Transactions on biomedical Engineering*, 2001, **48**(1), 96-104.

DIRECT PLASMA DIAGNOSTICS IN ELECTRON ACCELERATION EXPERIMENTS AT PW-CLASS PEARL FACILITY

K.F. Burdonov and **A.A. Soloviev**

Institute of Applied Physics, Russian Academy of Sciences
46 Ulyanov st., Nizhny Novgorod 603950, Russia
burdonov@appl.sci-nnov.ru

One of the most frequently used and effective methods of cancer disease treatments is electron therapy that is a kind of hadron therapy. Electron therapy is mostly employed for treating malignant tumors located at a depth of 1–6 cm from the skin surface (skin cancer, clay pipe cancer, cervical carcinoma, breast cancer, etc). The equipment used in electron therapy is bulky, hence, it is available only in conventional colliders. Therefore, recently active study of the physics of high peak power laser radiation interaction with plasmas is of great interest. When a high power laser pulse is focused on a gas jet target, effective acceleration of plasma background electrons to energies of hundreds MeV on the centimeter scale takes place through the LWFA mechanism [1, 2]. Compact size and relatively low cost of laser-plasma accelerators shows great promise for their effective use in medical laboratories. At the moment laser-plasma accelerators are at the stage of theoretical development and far from serial production. The major problem is achievement of electron bunches with maximum energy with low divergence and high experimental reproducibility. Information about laser produced plasma conditions is necessary for more detailed understanding of physical processes occurring in LWFA experiments. This work is devoted to indirect and direct plasma concentration diagnostics in LWFA experiments at PEARL [3]. PEARL is the PW-class laser facility in IAP RAS based on the principle of optical parametric chirped pulse amplification and producing 50 fs and 10 J laser pulses at 910 nm.

The main PEARL pulse is split into two parts by a transparent mirror before the interaction vacuum chamber, where laser-plasma interaction takes place. For detailed description of laser-plasma experiments and diagnostic at PEARL see references [4] and [5]. The powerful pulse then serves as a driver coming into the target chamber where it is focused on a supersonic gas jet by means of an off-axis parabolic mirror with f/15 or f/6 forming the focal spot sizes of the laser beam of 18 μm and 7.2 μm at FWHM intensity, respectively. The average laser intensities correspond to the normalized vector potential $a_0 = 2$ and $a_0 = 7$, respectively. The second part with a much lower power transmitted by the mirror comes into the diagnostic channel where it is used for the interferometric diagnostics of plasma density. The helium or nitrogen gas jet is formed with a specially designed supersonic conical nozzle with diameters of 2 mm, 5 mm, and 10 mm.

Indirect measurement of plasma density is performed by means of Michelson interferometer in one arm of which the gas jet is placed. The interference patterns are registered by a CCD camera. The inverse Abel transformation is also applied to the gas jet induced phase distortions to reconstruct the gas density profile. Three gas nozzles (2, 5 and 10 mm) are calibrated for helium and nitrogen gases in the range of backing pressure from 5 to 100 bar. The calibration shows that the nozzles produce flat-top gas density profiles with a plateau size of 1 mm, 3.5 mm and 8 mm for the 2, 5 and 10 mm diameter nozzles, respectively. A typical jet induced phase distortion and density profile at 1 mm above the nozzle edge for 10 mm gas jet are presented in Fig. 1(a, b).The calibration shows that the value of gas density depends linearly on the nozzle backing pressure for the range of 5 to 100 bar.

Direct measuring of plasma density by means of the Michelson interferometer was performed. The probe radiation that is a weaker femtosecond replica of the high-power pulse allows temporal resolution of the phase measurements on a femtosecond time scale. It should be noted that using this technique plasma density distribution can be measured correctly, if the plasma channel has axial symmetry. In fact, in a He gas jet the measured plasma density exceeds neutral density by a factor of 2, which means that He is fully ionized. This is in a good agreement with the fact that with the laser intensities of order 10^{19} W/cm^2 used in the experiment He gas should be fully ionized [6]. However, for N_2 gas jet the ionization degree depends on laser intensity and, hence, the plasma channel is strongly nonuniform in radial direction. Full ionization of nitrogen occurs only at laser intensities exceeding 10^{19} W/cm^2 [7]. According to this paper we expect five times ionized nitrogen for the focusing angle f/15 and fully stripped nitrogen plasma in experiment with f/6 focusing mirror. The resulting observations are presented in Fig. 1(c, d). One can see a plasma channel with the

corresponding plasma density $N_e = 7\times10^{18}$ cm^{-3} measured at 30 bar backing pressure and f/15 focusing. The neutral density N and the corresponding plasma density N_e for different nozzles at 10 bar backing pressure are given in Table 1.

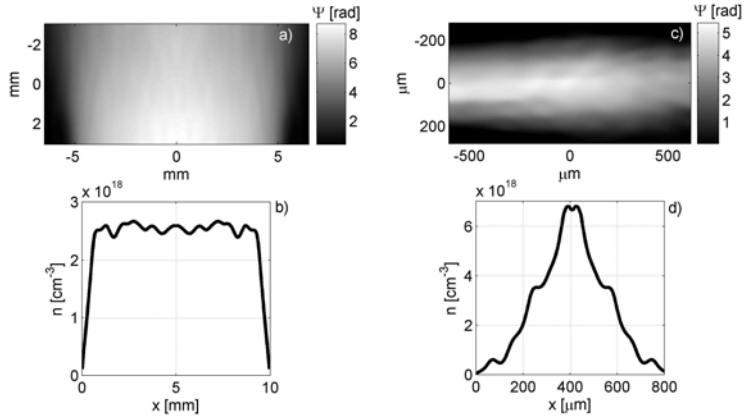

Fig. 1. Nitrogen jet induced phase distortions (a) and corresponding neutral density profile (b) for 10 mm nozzle at 100 bar of backing pressure; typical plasma channel phase distortions (c) and corresponding plasma density profile (d) for 10 mm nozzle and 40 bars of nitrogen backing pressure

Table. 1. Gas density and the corresponding plasma density for backing pressure of 10 bar

Nozzle diameter	N / N_e [1/cm^3], He	N / N_e(f/6) / N_e(f/15) [1/cm^3], N_2
2 mm	$1.8\cdot10^{18}$ / $3.6\cdot10^{18}$	$1.8\cdot10^{18}$ / $2.5\cdot10^{19}$ / $1.8\cdot10^{19}$
5 mm	$1.75\cdot10^{18}$ / $3.5\cdot10^{18}$	$1.5\cdot10^{18}$ / $2.1\cdot10^{19}$ / $1.5\cdot10^{19}$
10 mm	$2.5\cdot10^{17}$ / $5\cdot10^{17}$	$2.5\cdot10^{17}$ / $3.5\cdot10^{18}$ / $2.5\cdot10^{18}$

Direct and indirect measurements of plasma density profiles in LWFA experiments on PEARL facility are performed. Calibration plasma density quantities for nozzles 2, 5 and 10 mm for nitrogen and helium for f/6 and f/15 focusing are obtained.

References

1. S. Kneip et al., *Phys. Rev. Lett*., 2009, **103**, 035002.
2. D.H. Froula et al., *Phys. Rev. Lett*., 2009, **103**, 215006.
3. V. Lozhkarev et al., *Laser Phys. Lett*., 2007, **4**(6), 421-427.
4. A. Soloviev, K. Burdonov et al., *Nucl. Instr. and Meth. in Phys. Res. A*, 2011, DOI: 10.1016.
5. A. Soloviev, K. Burdonov et al., *Rew. Sci. Instr.*, 2011, **82**, 043304
6. B. Walker et al., *Phys. Rev. A*, 1993, **48**, R894.
7. S. Hulin et al., *Phys. Rev. E*, 2000, **61**, 5693.

EXPERIMENTAL CAPABILITIES OF LOW INTENSITY LASER RADIATION IN THE BLUE LIGHT RANGE

V.V. Chernov[1], **K.V. Kulakova**[2], and **T.G. Sherbatyuk**[2]

[1] Institute of Applied Physics RA, Nizhny Novgorod, Russia, kulakova-k@yandex.ru
[2] Nizhny Novgorod State University, Russia

The aim of the work is study of the biological effects of low intensity laser radiation (LILR) at the wavelength of 475 nm *in vitro* and *in vivo*. At the first stage we defined *in vitro* the presence and the extent of the impact of LILR on various biological liquids. At the second stage we estimated the influence of LILR on the organism of laboratory animals *in vivo.* The experiments were performed on male white nonlinear rats – healthy and with intertwined Pliss's lymphosarcome; 2 series of experiments with various modes of the influence of low intensity laser radiation were carried out.

At the first stage, experiments were performed on pools of plasma of blood of white nonlinear rats (normal and with experimental tumor: the term of growth of Pliss's lymphosarcome was 14 days), homogenate of the tumoral cells Pliss's lymphosarcome (LFS). The impact of LILR on the level of free-radical oxidation (the Method of induced hemoluminescence) and features of sample structure (the Method of wedge-shaped dehydratation [1]) was assessed. Results of the impact were recorded for 15 minutes immediately after irradiation.

At the second stage, 2 series of experiments were carried out on normal and LFS-transplanted rats with various modes of LILR impact. In the first series, starting from the 5th day after LFS cell transplantation the area of growing tumor was LILR irradiated with the duration of 1 minute for 10 days. In the second series of experiment, the area of growing tumor was irradiated starting on the 2nd day after its transplantation for 15 minutes, once a day. The animals without Pliss's LFS were irradiated by an analogous scheme. 14 days after tumor inoculation the blood sample was assessed for the action of LILR on the level of free-radical oxidation, structural features, concentration of the whole protein in plasma and glucose in the blood of the experimental animals. The influence of LILR on growth of the experimental tumor was also assessed. Light-optical microscopy was carried out on hematoxylin eosin stained paraffin histologic cuts of tumor [2]. The degree of tumor growth inhibition was calculated according to [3].

The most important conclusion is the following. *In vivo* LILR at the wavelength of 475 nm reduces the level of peroxidation in blood plasma, normalizes structuring of the peripheral zone of facies, and inhibits tumor growth and dystrophic changes in tumor tissue cells in the organism of animals with experimental tumor, independent of irradiation initiation and time.

References

1. V.N. Shabalin, S.N. Shatokhina, "A morphology of the biological liquids of human", M., Hrizostom, 2001, 304pp.
2. O.V. Volkova, Yu.K. Eletckiy, "The basis of the gistology with gistology technics", M. Medicine.
3. V.P. Fisenko, "The Manual on experimental (pre-clinical) to studying of new pharmacological substances", M., ZAO "IIA Remedium", 2000, 832 pp.

TEMPERATURE DYNAMICS OF CORTICOSTEROID HORMONES IN THz FREQUENCY RANGE

E.V. Fedulova[1], **I.N. Smirnova**[1], **A.V. Kargovsky**[1], **D.A. Sapozhnikov**[1], **M.M. Nazarov**[1], **O.P. Cherkasova**[2], and **A.P. Shkurinov**[1]

[1]Physics Department of M.V.Lomonosov Moscow State University, Moscow, Russia
fedulova@physics.msu.ru
[2]Institute of Laser Physics of the Siberian Branch of the Russian Academy of Sciences, Novosibirsk, Russia

The studied corticosteroids play a crucial role in many physiological processes in the human and animal organisms and their biological activity is implemented through their interaction with receptors and attributes to their structure. A challenging range for vibrational spectroscopy is presented by the terahertz (THz) frequency domain (0.1-10 THz or 3-300 cm^{-1}), corresponding to energies of a few meV. In the present work the complex transmission spectra of progesterone (PG) and 17α-hydroxyprogesteron (17-HP) have been measured by THz time-domain spectroscopy (THz-TDS) in the spectral range 15-85 cm^{-1} and in the temperature range 17-300 K.

Two corticosteroids have been chosen as the model molecular system: PG and 17 - HP, the latter presents the chemical modification of the former. These corticosteroids have very similar chemical structures (differ only by OH group while the total number of atoms is approximately the same), and also assemble into molecular crystals with the same crystal structures which allows us to isolate the influence of the intermolecular bonding on vibrational spectra, thus the changes of intermolecular arrangement were minimized as much as possible.

The aim of the present work was the investigation of PG and 17-HP temperature dynamics in THz frequency range. Also solid-state DFT calculations of positions and intensities of all observed bands were performed by $DMol^3$ (version 4.4) [1].

Those steroids have been investigated in detail by UV spectroscopy (10-400 nm) and IR spectroscopy (4000-400 cm^{-1}). We started the first spectroscopic studies of steroid hormones in THz frequency range recently [2]. Our typical THz-TDS [3] apparatus has been reported previously [4] and it is modified with cryostat for reducing the sample temperature down to 10 K. The substances were purchased from Koch-Light Laboratories Ltd, UK, and used without further purification. The samples were prepared by pressing the pure polycrystalline powder to disks of thickness 0.4 mm, diameter 5 mm and density 1.2 mg/mm^3 by applying a pressure about 50 MPa. The presented corticosteroids exist in the form of molecular crystals of the same orthorhombic space group $P2_12_12_1$ with 4 molecules per unit cell.

The molecules of progesterone assemble into the crystal unit cell with minimal for the two provided substances volume, i.e. with maximal molecular packing and are bounded with each other by van der Waals forces. It should lead to appearance of high-Q collective lattice vibrations in absorption spectra. At 300 K we observe the set of "narrow" (about 5 cm^{-1}) bands for absorption spectra (Fig.1a). Upon cooling it became possible to resolve more absorption peaks, and the blue shift is observed. The displacement of the peaks with temperature can be fitted by linear dependence with different coefficients. But two bands (40.7 and 44.1 cm^{-1}) reveal the anomalous red shift at temperatures below 60 K. This kind of red shift was reported previously [5] and it was explained by the competition of intra- and intermolecular forces.

The molecule of 17-HP differs from a molecule of PG only by one hydroxyl group at the 17 carbon position. This change of the structure leads to the appearance of an additional hydrogen bond between the molecules [6] and unit cell volume increases. The experimental THz absorption spectrum of 17-HP comprises only two well defined peaks at 53.2 cm^{-1} and 65.5 cm^{-1} at room temperature. In contrast to progesterone, the peaks of 17-HP THz absorption spectrum don't shift noticeably but only sharpen with temperature decrease. (Fig. 1b), but the bands get narrow upon cooling that allows resolving more peaks. This behavior can be explained by specific role of hydrogen bonds connecting the layers in the 17-HP crystal.

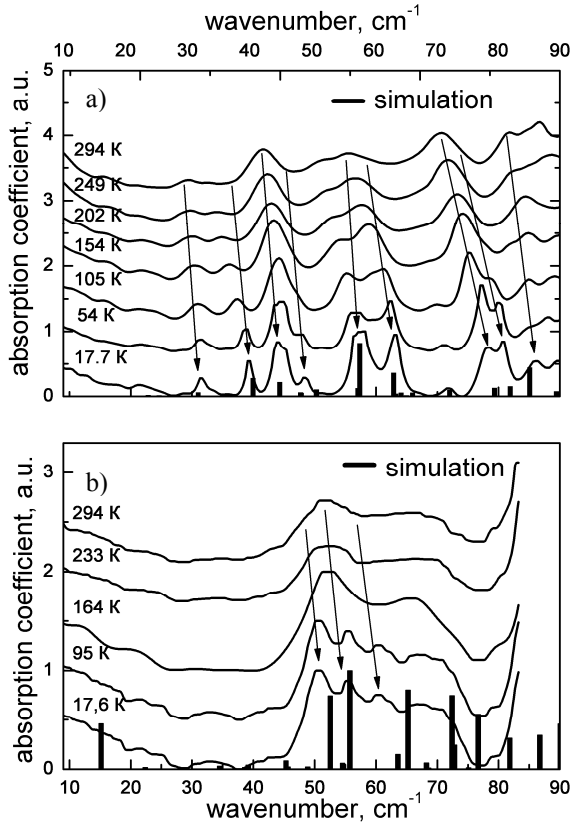

Fig. 1. Absorption spectra. a) measured PG spectra (solid lines) and calculated frequencies with their relative intensities (bars), b) similarly for 17-HP. The spectra are offset for clarity

The results of theoretical simulation of all observed bands are shown in Fig as vertical lines. Due to taking into account the unit cell of the molecular crystal, but not isolated molecule as before [7], successful agreement with experiment allows to assign both intra- and intermolecular bands of the molecular crystal.

In conclusion: the absorption spectra in THz frequency range are found to be sensitive to small structure changes of the molecules and to the presence of intermolecular hydrogen bonds while spatial symmetry is preserved. The frequencies of observed intra- and intermolecular bands are not constant and independent, but are rather influenced by each other, as well as by the temperature and the mass of molecules involved. The different temperature dynamics of the THz band positions and intensities with decreasing temperature were observed and analyzed. The appearance of hydrogen bonds reveals in red- shift of ranges of different vibrations. Also we can see that the frequency ranges of different type vibrations are limited in frequency.

References

1. B. Delley*, J. of Chem. Phys.,* 2000, **113**, 7756-7764.
2. I.N. Smirnova, E.V. Fedulova at al., *Vestnik Novosib. Univ.: Phisica*, 2010, **4**, 171-175.
3. X.-C. Zhang and J. Xu, *Introduction to THz Wave*, Photonics© Springer Science+Business Media, LLC 2010.
4. M.M. Nazarov, A.P. Shkurinov, E.A. Kuleshov, V.V. Tuchin, *Quant. Elect.,* 2008, **38**, 647-654.
5. M. Walther, B. Fischer, M. Schall at al., *Chem. Phys. Lett*., 2000, **332**, 389-395.
6. N.N. Brandt, A.Y. Chikishev, M.M. Nazarov at al., *Vib. Spectrosc*., 2008, **47**, 53-58.
7. M.B. Johnston, L.M. Herz, A. L.T. Khan at al., *Chem. Phys. Let.t,* 2003, **377**, 256-262.

Invited

ADVANCED CONTACT AND NON-CONTACT SOFT TISSUE SURGERY WITH DIODE LASERS

F. Feldchtein[1], **K. Magid**[2], **A. Belikov**[3], **A. Scrypnic**[3], and **G. Altshuler**[1]

[1] Dental Photonics, Inc., Walpole MA USA, felixfel00@yahoo.com
[2] Private practice Harrison NY USA,
[3] Saint Petersburg State University of Information Technology, Mechanics and Optics, Saint Petersburg, Russia

Introduction and Aim of the Study

Mechanism of action and light-tissue interaction for soft tissue laser surgery in the near infrared spectral range remains a controversial issue in the literature. The role of tissue absorption and scattering for the laser radiation, as well as ability to cut tissue using direct laser radiation alone remains a topic for debates.

The aim of this study is clarification of the mechanisms and processes involved in contact and non-contact soft tissue surgery with near infrared diode lasers. We analyze and discuss problems of contact and non-contact diode laser surgery. We are also presenting experimental results of laser surgery using the concept of thermo-optical tip and automated power control (APC).

We performed numerical simulation of non-contact and contact cutting processes. The model includes Monte-Carlo simulation of light propagation in a fiber tip (initiated or not) and mucosa, heat transfer equation for calculation of heat production in the tip and tissue. The temperature distribution in the tip and tissue was calculated and coagulation zone was defined using Arrhenius integral. This model takes into account the effect of tissue coagulation due to direct laser light absorption, heat conduction from the optical tip heated by laser light, and heat radiation of the tip. In the experimental part we are using a proprietary laser diode pulsed surgical system with the wavelength of 980 nm, average power up to 25 W, fiber delivery with 400 um fiber core diameter. The experiments were performed *ex vivo* using fresh tissue samples. The tangential force necessary to perform cutting at predetermined depth and speed was recorded. Coagulation depth was visualized and measured using express histology with lactate dehydrogenase (LDH) staining. The system implemented an automated power control algorithm; the laser power was dynamically adjusted to maintain predetermined tip temperature. The cutting force and coagulation was compared for the new system with APC and traditional laser surgical system with fixed power delivery. Computer-controlled speed of movement of the tip was in the range of 0.8-12 mm/s.

Results

Both computer simulation and in vitro experiments confirmed that direct cutting with laser light alone requires high power, beyond the capabilities of existing dental diode lasers. For the diode lasers with moderate power the only practical cutting mechanism is contact surgery with a hot initiated tip. Automated power control is providing significantly more consistent cutting and less collateral damage zone than fixed power. The collateral damage remains constant with speed of cutting changing in a broad range from 0.8 to 12 mm/s. APC reduces tip degradation and collateral tissue damage.

Discussion / Conclusion

Contact surgery with hot tip is a dominating mechanism of diode laser surgery in the near infrared range. Direct non-contact cutting with laser power alone requires high power level beyond capabilities of diode lasers available for dentistry.

Automated power control can provide faster, safer diode laser surgery minimizing collateral tissue damage and making it practically independent of cutting speed which significantly decreases the risk of side effects.

Invited

LASER-TISSUE SOLDERING USING ICG LOADED SILICA NANOSHELLS

D.S. Schöni[1], S. Bogni[2], A. Wirth[3], I. Vajtai[4], U. Pieles[3], M. Reinert[1], and **M. Frenz[2]**

[1] Department of Neurosurgery, Inselspital Bern, University of Bern, Switzerland
[2] Department of Biomedical Photonics, Institute of Applied Physics, University of Bern, Switzerland
frenz@iap.unibe.ch
[3] Department of Chemistry and Bioanalytics, Academy for Life Sciences, Muttenz, Switzerland
[4] Section of Neuropathology, Institute of Pathology, University of Bern, Switzerland

Laser tissue soldering (LTS) has been under investigation for tissue fusion in general and in particular for vascular anastomosis for several years [1–3]. Laser soldering is defined as heating an absorbing tissue solder which is placed inbetween or on the surface of the two tissue edges to be fused together. LTS is a very promising technique which provides fast and watertight tissue fusion with fewer traumas and no foreign body reaction. It can be applied for different vessel sizes and intraoperative locations both in an open operation as well as endoscopically. Still, there are some serious problems limiting its general clinical applicability. Our experiments have shown that the strength of a soldered tissue connection strongly correlates with the maximum temperature reached during the laser irradiation [4]. Therefore, precise temperature control is one of the major hurdles to be solved in LTS. The key to a successful laser tissue fusion is a homogenous energy deposition resulting in a denaturation of proteins which finally leads to the demanded tensile strength and bursting resistance [5-7]. The main drawback of a liquid solder is the high mobility of the absorbing chromophore during the soldering procedure. Liquid solder tends to flow off during soldering. The dilution of the absorbing chromophore thus changes the amount of absorbed energy, which leads to irreproducible temperatures and strong quality variances of the soldering result. In addition, it was shown that liquid ICG can leak into the vessel lumen during the laser irradiation, which causes severe damage of the intima and immediate thrombosis.

A first improvement was made when introducing a solder carrier material (polymer scaffold), which, in a dried state, provides almost complete fixation of the liquid protein-chromphore solder thus improving the reproducibility [2]. Although leaking out of the solder could strongly be reduced, our *in-vivo* experiments revealed that the completely dried ICG and albumin doped PCL-scaffold lacks pliability and is therefore not convenient for microsurgical procedures. Almost none of the soldered vessels using the dried scaffold could be sealed. If on the other hand using the scaffold in a wet or semi-wet condition, which keeps the scaffold nicely flexible, it unfortunately provides only partial fixation of the chromophore. Part of the liquid solder still leaks out of the scaffold when the scaffold caused by laser heating starts to melt and shrinks.

A further step of improvement was the quantification and prediction of the energy deposition precisely at the intended location. This step was done by applying nanotechnology. We encapsulated the absorbing ICG into silica nanoshells which could directly be bound to the porous structure of the PCL polymer scaffold in which the albumin solder was administered. The ICG nanoshells have a diameter of 250 – 270 nm.

An overview of a nanoshell scaffold surface viewed by scanning electron microscopy shows its pore morphology (Fig. 1A). High resolution magnification (Fig. 1B) reveals incorporated and surface adhered nanoshells.

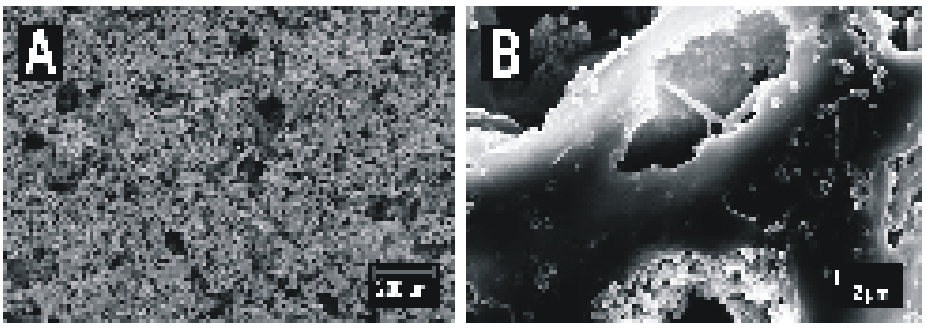

Fig. 1. Scanning electron microscopy pictures of a nanoshell scaffold. A: Overview of a nanoshell scaffold. B**:** Close-up view showing the incorporated nanoshells inside the PCL scaffold

15 arteries have been successfully soldered using the nanoshell-soldering and 14 artery fusion were created using the classical soldering technique without nanoparticles. In both cases the ICG concentration was fixed such that the absorption coefficient of the scaffolds was exactly the same.

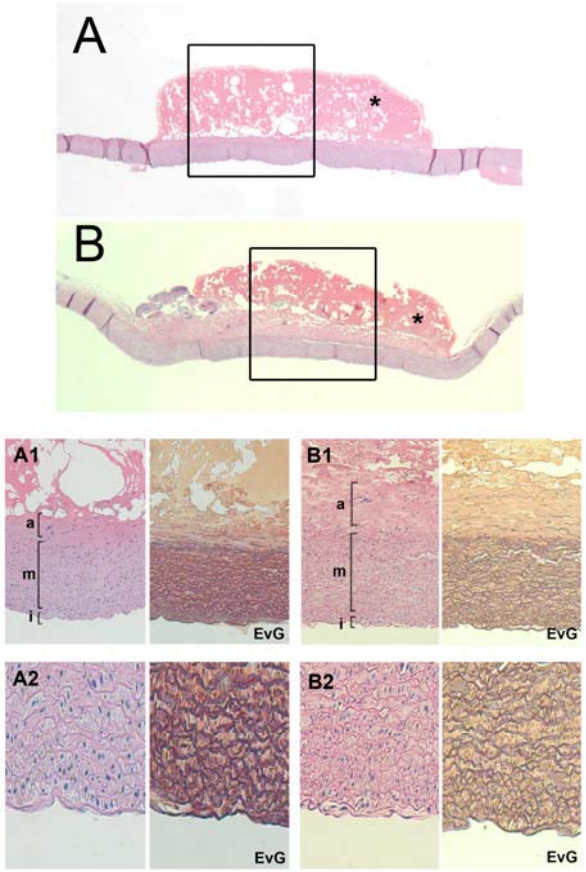

Fig. 2. Microphotographs of vessel wall document type and extent of thermal-induced alterations entailed by the soldering procedure. In series (A) results of conventional soldering technique are depicted, while series (B) show those obtained by nanoshell soldering. A, B: Scanning view of longitudinally sectioned rabbit aorta shows crust-like layer of coagulated scaffold (*) adherent to the adventitia. A1, B1: Detail view of soldered aortic wall architecture corresponding to boxed areas in (A) and (B). The tunica media (m) accounts for most of the breadth of the vessel wall, and will be readily identified by its parallel arrays of elactic fibers. The adventitia (a) tends to gradually merge into the periaortic connective tissue. Using these soldering parameters (3.07 W and 30 s), in both groups thermal damage to the adventitia – as evidenced by disappearance of nuclear staining – can clearly be seen. Liquified scaffold substance is felt to permeate through the dissociated outermost connective tissue elements of the adventitia. A2, B2: Details view of the intima (i) comprised of an endothelial cell layer. Note the largely intact-appearing nuclear staining as well as lack of fragmentation of elastic fibers. No thermal-induced alterations to the intimal layer were recognized. Photomicrographs not labeled otherwise represent H&E stained sections.
Original magnification: (A, B): x15, (A1, B1): x100, (A2, B2): x120

In all cases the rupture took place at the interface between the vessel wall and the scaffold. The mean tensile strength of the nanoshell tissue fusion technique was 734 ± 327 mN (median = 640 mN), which is slightly higher compared to the classical solder technique with a mean of 649 ± 389 mN (median = 545 mN). However, the comparison of means using a non parametric test (Wilcoxon) yielded no significant difference in tensile strength ($p = 0.42$).

Although the comparison of the temporal temperature development revealed an identical course, the statistical analysis showed for the nanoshell group a significant less variance (Levene test for homogeneity of variance: $p = 0.03$) at maximum temperature.

The histological results (see Fig. 2) show that the laser-induced heating effect mediated by the use of nanoshells allows us (i) the spatial extent of tissue alterations to be planned and/or controlled, (ii) the severity of heat-induced tissue damage to be kept below levels of generalized irreversible cellular

injury within the mechanically most relevant layer of the arterial wall (tunica media) and (iii) the supporting extracellular matrix framework (in particular elastic fibers) to remain largely unaffected so as to foster cellular regeneration.

ICG silica nanoshell tissue soldering is a novel and potent soldering technique with improvement in temperature characteristics and therefore in tissue preservation. Delicate functional structures such as the intima and endothelium can be protected as shown in the histological assessment. Nanotechnology enables for the first time a quantitative prediction of laser tissue soldering, with future improvement options such as covalent and gradient specific embedding into the solder polymer structure. By using nanotechnological refinements laser tissue soldering has further stepped toward clinical application.

Acknowledgements. This work was supported in part by the Swiss Commission of the Encouragement of Scientific Research Nr. 11478.1pfls-ls.

References

1. L.S. Bass, M.R.Treat, *Lasers Surg. Med*., 1995, **17**(4), 315-349.
2. B. Ott, M.A. Constantinescu, D. Erni, A. Banic, T. Schaffner, M. Frenz, *Lasers Surg., Med*., 2004, **35**(4), 312-316.
3. W.Z. Yahr, K.J. Strully, E.S. Hurwitt, *Surg. Forum*, 1964, **15**, 224-226.
4. S. Bogni, O. Stumpp, M. Reinert, M. Frenz, *J. Biophotonics*, 2010, **3**(5-6), 284-295.
5. K.M. McNally, B.S. Sorg, E.K. Chan, A.J. Welch, J.M. Dawes, E.R. Owen, *Lasers Surg. Med*., 1999, **24**(5), 319-331.
6. K.M. McNally, B.S. Sorg, E.K. Chan, A.J. Welch, J.M. Dawes, E.R. Owen, *Lasers Surg. Med*., 2000, **26**(4), 346-356.
7. A. Bregy, S. Bogni, V.J. Bernau, I. Vajtai, F. Vollbach, A. Petri-Fink, M. Constantinescu, H. Hofmann, M. Frenz, R.M. Solder, *Lasers Surg. Med*., 2008, **40**(10), 716-725.

ANALYSIS OF PROBLEMS IN PDT OF SKIN CANCER AND THEIR POTENTIAL SOLUTION BASED ON CLINICAL RESULTS

S.V. Gamayunov [1], **R.R. Kalugina**[1], **V.V. Slugarev** [1], **A.N. Denisenko**[1], and **N.M. Shakhova** [2]

[1] Regional Oncological Hospital, Nizhny Novgorod, Russia, guznood@pochta.ru
[2] Institute of Applied Physics RAS, Nizhny Novgorod, Russia

Skin cancer is still a topical problem of modern oncology. The tendency towards an increase of the number of such pathologic cases is apparent. 39.5 skin cancer cases per 100.000 inhabitants recorded in Russia make it the second most frequently encountered malignant disease in this country and in the Nizhny Novgorod region it ranks first.

The main techniques for skin cancer treatment are radiation therapy and operative surgery. At the same time, oncologists face a number of problems when applying these standard techniques. This concerns primary multifocal skin tumors and tumors localized in complex anatomic areas such as face, eye corners, dorsum of nose, auricle, acoustic meatus. The procedure of radiation therapy is complicated by complex field configuration and possibility of damaging neighboring structures (for example, eye). Surgery in such cases is usually accompanied by cosmetic defects. Another problem which has not received a proper solution yet is skin tumor recurrence after full course of radiation therapy or previous surgery.

One of modern and most perspective techniques for skin tumor treatment is photodynamic therapy (PDT) [1]. Damage to malignant cells is produced by photochemical reaction induced by interaction of photosensitized selectively accumulated in the tumor [2,3] and laser radiation at a corresponding wavelength. Among the advantages of this technique are local character of impact, possibility for formation of complex-shaped fields, high safety, and absence of threshold and cumulative factors limiting repetitive application. At the same time, optimal dose of laser radiation is to be defined; predictors of disease recurrence, recurrence prevention techniques and indications for combinations with other techniques are not sufficiently studied.

Materials and methods

Photodynamic therapy of skin cancer has been used at the Nizhny Novgorod oncologic dispensary since August 2007. 73 patients have been treated by now. Patient distribution over the main tumor types is presented in Table 1.

Table 1

Tumor type	case frequency X%(m out of n cases)
Primary skin cancer	79% (58 out of 73 cases)
Recurrent skin cancer	21% (15 out of 73 cases)
Single focus	74% (54 out of 73 cases)
Multiple foci	26% (19 out of 73 cases)
Basal-cell carcinoma	85% (62 out of 73 cases)
Squamous cell carcinoma	15% (11 out of 73 cases)

Photoditazine produced by VETA-GRAND Co. or radachlorine produced STADA were used as photosensitizers. Photosensitizers doses were calculated in accordance with patient's weight as Me{min;max}= 0.9{0.75;1.15} mg per kg of body weight.

Laser irradiation was performed by Atkus-2 setup equipped with semiconductor laser at the wavelength of 662 nm. Average power density was 0.4 W/cm^2 varying from minimal value of 0.35 W/cm^2 up to maximal value of 0.5 W/cm^2. Higher power densities were not applied due to appearance of pain syndrome. Average laser radiation dose was 250 J/cm^2. Minimal dose for primary small-size basal-cell cancers without infiltrative component was 100 J/cm^2, maximal dose at recurrent squamous cell carcinoma and large tumors reached 350 J/cm^2.

Results

Full response after single PDT session is observed in 86% (63 out of 73 cases) of patients. Partial response manifested by tumor decrease for more than 50% is observed in 11% (8 out of 73 cases) of patients, while the absence of effect is registered in 3% (2 out of 73 cases). For 4 patients with partial response the repeated PDT session with increased dose was performed resulting in full response. Four patients with partial response and two patients with no response were treated by surgical tumor excision.

During follow up from 2 to 32 months the recurrence appeared in 15% (11 out of 73 cases) of patients. For 8 patients the repeated PDT session was performed resulting in full response. For 3 patients surgical treatment was performed.

Analysis of recurrent reasons has shown that in 5 patients the continuation of tumor growth occurred in the periphery of tumors which is likely to be connected with incorrect irradiation area choice. In 6 patients the continuation of tumor growth occurred in the focus after therapy applied to large (>5 mm) foci, which is probably connected with incorrect irradiation dose choice. Analysis of the dependence of recurrence frequency on tumor type is presented in Table 2.

Table 2

Tumor type	Recurrence frequency X%(m out of n cases)
Primary skin cancer	9% (5 out of 58 cases)
Recurrent skin cancer	40% (6 out of 15 cases)
Basal-cell carcinoma	11% (7 out of 62 cases)
Squamous cell carcinoma	36% (4 out of 11 cases)

Conclusion and discussion

Photodynamic therapy is a convenient, safe and effective technique for skin cancer treatment. Considering the problem of recurrence after performed treatment several issues should be accounted for. Continued growth at the periphery is connected with incorrect choice of irradiation field shape, which makes essential non-invasive diagnosis of tumor boundaries, in particular, by the OCT technique. Tumor recurrence in scar, squamous cell structure and pronounced exophytic or infiltrative component can be estimated as predictors of high recurrence risk. In these cases increase in irradiation dose, control of photosensitizer accumulation level by fluorescent analysis and early application if combined treatment techniques (PDT+surgical treatment or PDT+radiation therapy) should be considered.

Acknowledgements

The authors appreciate the financial support from the Russian Foundation for Basic Research (08-02-99049-р_офи, 11-02-00916-а) and the Presidium of the Russian Academy of Sciences. The authors are also grateful to the staff and management of the Nizhny Novgorod Regional Oncological Hospital for the possibility to conduct this study.

References

1. J. Moan, Q. Peng, "An outline of the history of PDT", in Thierry Patrice. *Photodynamic Therapy*. Comprehensive Series in Photochemistry and Photobiology. **2**. The Royal Society of Chemistry, 2003, pp. 1–18. doi:10.1039/9781847551658.
2. T.H. Foster, B.D. Pearson, S. Mitra, C.E. Bigelow, *Photochemistry and Photobiology,* 2005, **81**(6), 1544-1547; doi:10.1562/2005-08-11-RN-646.
3. J.D. Wilson, C.E. Bigelow, D.J. Calkins, T.H. Foster, *Biophysical Journal* (Biophysical Society), 2005, **88**(4), 2929–2938; doi:10.1529/biophysj.104.054528.

LASER PATTERNED MICROCOAGGULATION (LPM) TREATMENT OF GINGIVAL PATHOLOGY. PILOT CLINICAL STUDY

N. Gladkova[1], F. Feldchtein[2], Yu. Fomina[3], M. Karabut[4], A. Muraev[3]
A. Belikov[5], A. Skrypnik[5], E. Zholobova[5], K. Shatilova[5], I. Zabezhinskaya[6],
D. Popov[7], E. Kiseleva[1], and **E. Gubarkova[1]**

[1] Institute of Applied and Fundamental Medicine, Nizhny Novgorod State Medical Academy, Russia
natalia.gladkova@gmail.com
[2]Dental Photonics Inc., MA, USA
[3]Nizhny Novgorod State Medical Academy, Russia
[4]Nizhny Novgorod Lobachevsky State University, Russia
[5] St.-Petersburg State University of Information Technologies, Mechanics, and Optics, Russia
[6] Dental Polyclinic №29, Russia
[7] Dental Clinic TUSFILD, Russia

Background and Objective

Tissue coagulation stimulates intensive healing response, which can result in a therapeutic effect. A minimally invasive microsurgical approach has been used for Laser Patterned Microcoagulation (LPM) to initiate gingival or oral mucosa tissue healing. This LPM treatment concept is similar to the use of fractional photothermolysis [1] or lattice of optical islets [2], which has been successfully applied in dermatology [1,3] and ophthalmology [4].

Study Design

Thirty-three patients with periodontitis (depth of periodontal pockets more than 3.5 mm) and thirteen patients with gingivitis were enrolled in the multicenter split-mouth study. Every patient received a single treatment in multiple extrasulcular locations of gingiva with a diode laser operating at 980 nm wavelength and generating up to 20 W of power. Each single column of tissue microcoagulation was created by applying a tip 400 µm or 600 µm in diameter and irradiating the tissue through the tip with a single 150 ms pulse. Scaling & Root Planning (SRP) was performed in treatment and control quadrants of the oral cavity. We monitored 10 clinical parameters and indices of gingiva, including gingival index (GI), bleeding on probing (BOP), probing depth (PD), clinical attachment level (CAL). One patient with local spots of gingival hyperpigmentation received two consecutive treatments of these spots. For this patient we qualitatively monitored pigmentation level.

Results

Results of the treatment of patients with periodontitis are presented in fig. 1. Observation 3–6 months after a single treatment with the LPM technique showed a significant decrease in the depth of periodontal pockets (probing depth (PD), $p = 0.015$) and decrease of clinical attachment level (CAL, $p = 0.019$) in the treatment group compared with controls.

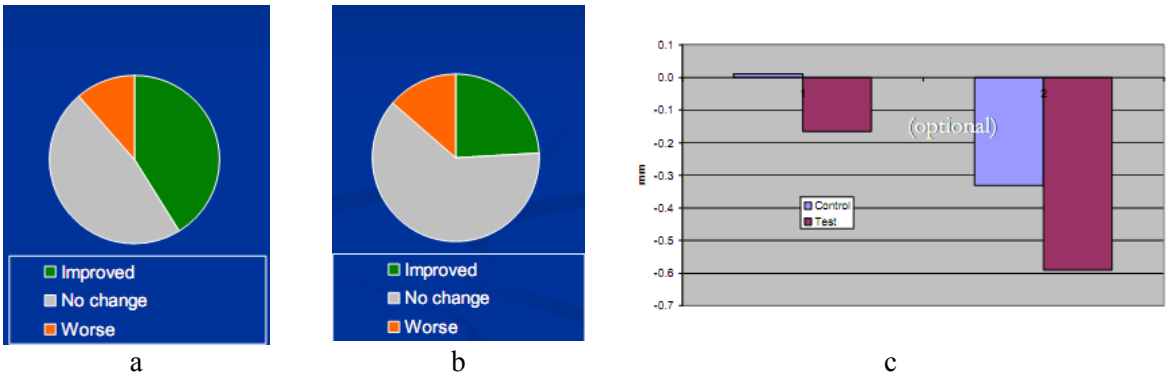

a b c

Fig. 1. Patients with periodontitis: probing depth change between baseline and 3 months follow up. Treatment quadrants (a); control quadrants (b). Change in PD (left) and CAL (right): baseline – 3 months (c)

8 of 13 patients had pronounced improvement of gingival index (GI) and bleeding on probing (BOP) (fig. 2) already 2 weeks after a single treatment; in the control groups the improvement was less pronounced but no significant statistical difference was revealed ($p > 0.05$). The improvement persisted for at least 3 months in both the groups.

a b c

Fig. 2. Treatment of a patients with moderate gingivitis:
(a) preoperative view, (b) immediately after LPM treatment, (c) 3 months after LPM treatment

The first clinical case of hyperpigmentation treatment using LPM demonstrated feasibility of a new, minimally invasive and effective method of localized gingival hyperpigmentation removal. The patient's discomfort was significantly less than that reported for other methods of depigmentation (Fig. 3).

a b c d

Fig. 3. Close up view of the pigmented spot: (a) preoperative view, (b) 2 weeks after the first LPM treatment, (c) 2 weeks after the second LPM treatment, (d) two months after the first LPM treatment

Conclusion

A treatment with the LPM technique induces a healing response in oral mucosa, showing LPM potential for oral mucosa and gingival regeneration. Complete healing was observed 3 months after the treatment with no keratinization change or scar tissue formation.

Acknowledgements

This work was supported by the Russian Foundation for Basic Research (project 10-02-01175), and the State Contract of the Russian Foundation No. 02.740.11.5149 and the grant of the Government of the Russian Federation (Contract No. 11.G34.31.0017). The authors are grateful to Dental Photonics, Inc (Walpole, MA, USA) for the support of this work.

References

1. D. Manstein, G.S. Herron, R.K. Sink, et al., *Lasers Surg. Med.,* 2004, **34** (5), 426-438.
2. G. Altshuler, M. Smirnov, and I.Yaroslavsky, *J. Phys. D-Appl. Phys.,* 2005, **38**(15), 2732-2747.
3. M.H. Jih and A. Kimyai-Asadi, *Semin. Cutan. Med. Surg.,* 2008, **27**(1), 63-71.
4. Y.M. Paulus, A. Jain, R.F. Gariano, et al., *Invest Ophthalmol. Vis. Sci.,* 2008, **49**(12), 5540-5545.

PERSPECTIVES OF PDT OF VULVA DISEASES

E.V. Grebenkina[1], **O.V. Kachalina**[2], **S.V. Gamayunov**[1], **O.V. Onoprienko**[1], **N.A. Illarionova**[1], **A.N. Denisenko**[1], **R.R. Kalugina**[1], and **N.M. Shakhova**[3]

[1] Regional Oncological Hospital, Nizhny Novgorod, Russia, gelena1980@mail.ru
[2] State Medical Academy, Nizhny Novgorod, Russia
[3] Institute of Applied Physics RAS, Nizhny Novgorod, Russia

Vulva cancer is the 4th most common type of cancer in the structure of oncogynecological diseases [1]. Its prevalence among malignant tumors of female reproductive organs is 5–8%. Vulva cancer is usually preceded by various background and precancer diseases. The problem of background and precancer diseases treatment still remains topical due to insufficient efficiency of existing treatment techniques, long duration of the disease and its severity, as well as due to high probability of malignization (20–30% vulva cancer cases are accompanied by displasia background) [1, 2]. The possibility of prevention of malignant tumor progress by treatment of background and precancer vulva diseases force oncologists to develop new methods of diagnostics and treatment of vulva diseases. Despite the wide variety of currently applied methods (conservative methods, cryodestruction, laser vaporization, surgical treatment), their efficiency still remains comparatively low. Existing medicinal methods do not ensure full elimination of local morphological alterations, do not provide long-term remissions, and require long treatment periods. Application of cryodestruction, laser vaporization or surgery induces scar deformation of vulva. Low-intensity laser therapy is one of the safest techniques, however its efficiency is insufficient because it does not provide stable result, and frequent recurrences require application of repetitive courses [3, 4].

Treatment of background and precancer diseases aimed at preventinng vulva cancer should be, on the one hand, rather radical and, on the other hand, preserving in order to ensure life quality of patients by maintaining reproductive and sexual functions. In this connection treatment techniques combining optimal treatment effect and prevention of complications are currently developed. One of modern perspective techniques for background and precancer vulva diseases treatment is photodynamic therapy (PDT). In this paper we present our pilot study on PDT application for vulva diseases treatment.

Materials and methods

Application of PDT for treatment of vulva background and precancer diseases was started in Nizhny Novgorod Regional Oncologic Dispensary in 2011. To date 3 patients have been treated: one with vulva lichen sclerosus, and two with squamous cell vulva hyperplasia. In all patients vulva pathologies were treated for a long period employing all existing methods, including surgery (vulvectomy) in one patient. PDT was performed using chlorine-derivative photosensitizer "Photoditazine" (Veta-Grand, Russia) in the dose of 1 mg/kg, which was injected intravenously with 200 ml of saline solution during 30 minutes. Laser irradiation was performed under general anesthesia or spinal anesthesia 1.5-2 hours after injection. Atkus-2 setup equipped with a semiconductor laser at the wavelength of 662 nm was employed. Laser irradiation was performed through monofiber quartz waveguides with a microlens on the operating part for delivery of radiation to all visible zones of pathologic process and surrounding tissues. The total dose of light energy in the areas with precancer process was 150-200 J\cm^2 and power density was 0.9–1 W\cm^2. The dose of light energy for other organ surfaces was 70–100 J\cm^2 and power density was 0.5–0.7 W\cm^2.

In the present work we estimated immediate results of the treatment. The obtained results were assessed by means of clinical monitoring, vulvoscopy, cytological and morphologic (biopsy) data. Analysis of long-term results is not available yet because follow-up of the treated patients is rather short (2 months).

Results

When assessing immediate results at the current stage of study we analyzed the course of post-operation period epithelization times. Worth mentioning is the pain syndrome manifested in the area of vulva during PDT which required narcosis application for adequate pain relief. The course of early post-operation period was accompanied by pain syndrome and required application of anesthetics for

the first two days. As a response to intensive light impact pathomorphosis of the area of pathologically changed vulva was accompanied by hyperemia and edema during the first two days followed by development of ulceration in 3–5 days. Epithelization of the specified areas started 7–10 days after the treatment and was completed in 3–4 weeks. In normal areas of vulva with less intensive light impact clinical changes manifested by hyperemia and edema were observed for 7–10 days after the treatment followed by relaxation in 14–15 days.

Full regression of pathologic processes in vulva in all patients was registered as a result of the performed treatment. No cases of unforeseen reactions or post-operation complications were observed, which allowed conservative management of post-operation period without additional procedures or medication support.

Conclusion

The reported stage of this study enables us to make only preliminary conclusions. First of all, our first experience confirmed that effective anesthesia is reasonable during PDT procedure and in the early post-operative period. Conservative postoperative management is warranted by absence of complications. We conclude that PDT being radical but careful is a method of choice for treatment of background and precancer vulva diseases.

Acknowledgements

The authors thank the Russian Foundation for Basic Research (11-02-00916-a) and the Presidium of the Russian Academy of Sciences for the financial support of this work. The authors are also grateful to the staff and management of the Nizhny Novgorod Regional Oncological Hospital for the possibility to conduct this study.

References

1. M. Ascencio, P. Collinet, M. Cosson, D. Vinatier, S. Mordon, "The place of photodynamic therapy in gynecology", *Gynecol Obstet Fertil*., 2007, Nov; **35**(11), 1155–1165. Epub 2007, Oct 22.
2. A. Juarranz, P. Jaen, F. Sanz-Rodriguez, J. Cuevas, S. Gonzalez, "Photodynamic therapy of cancer. Basic principles and applications", *Clin. Transl. Oncol*., 2008, Mar, **10**(3), 148-154.
3. M.A. MacCormack, "Photodynamic therapy in dermatology: an update on applications and outcomes", *Semin. Cutan. Med. Surg*., 2008, Mar, **27**(1), 52-62.
4. B.C. Wilson, M.S. Patterson, "The physics, biophysics and technology of photodynamic therapy", *Phys. Med. Biol*., 2008, May, 7; **53**(9), R61–109. Epub 2008, Apr 9.

Invited

LOW LEVEL LIGHT THERAPY FOR TRAUMATIC BRAIN INJURY

W. Xuan[1,2,3] Y. Y. Huang[1,2,4], Q. Wu[1,2,5], T. Ando[1,6], T. Xu[1,2,7], S.K. Sharma[1], G.B. Kharkwal[1,2], and **M.R. Hamblin[1,2,8]**

[1] Wellman Center for Photomedicine, Massachusetts General Hospital, Boston, MA, USA
e-mail Hamblin@helix.mgh.harvard.edu
[2] Department of Dermatology, Harvard Medical School, Boston MA, USA
[3] Traditional Chinese Medical University of Guangxi, Nanning, China
[4] Aesthetic and Plastic Center of Guangxi Medical University, Nanning, China
[5] Department of Burns and Plastic Surgery, Jinan Central Hospital Shandong University, Jinan, China
[6] Department Electrical Engineering, Keio University, Yokohama, Japan
[7] Laboratory of Anesthesiology, Jiaotong University, Shanghai, China
[8]Harvard-MIT Division of Health Sciences and Technology, Cambridge, MA, USA

Traumatic brain injury (TBI) is caused by falls, motor vehicle accidents, and violence. The major consequences of head injury include skull fractures, intracranial hemorrhages, elevated intracranial pressure, and cerebral contusion. Severe and moderate TBI, accidental or inflicted, is a major health and socio-economic problem throughout the world, especially in children and young adults. Despite promising preclinical data, most of the trials for TBI that have been performed in recent years have failed to demonstrate any significant improvement in outcome [1]. Because of this disappointing state of affairs, a plethora of experimental therapies that are not based on standard pharmaceutical agents have been investigated [2], including several physical treatments [3].

Low-level laser (light) therapy (LLLT) also known as "photobiomodulation" is an emerging therapeutic approach in which cells or tissues are exposed to low-levels of red and near infra-red light. Its experimental applications have broadened to include serious diseases such as heart attack [4], stroke [5], spinal cord injury [6]. LLLT may have beneficial effects in the acute treatment of TBI by increasing respiration in the mitochondria, causing activation of transcription factors, reducing key inflammatory mediators, inhibiting apoptosis, stimulating angiogenesis, and increasing neurogenesis [7] as shown in Fig 1.

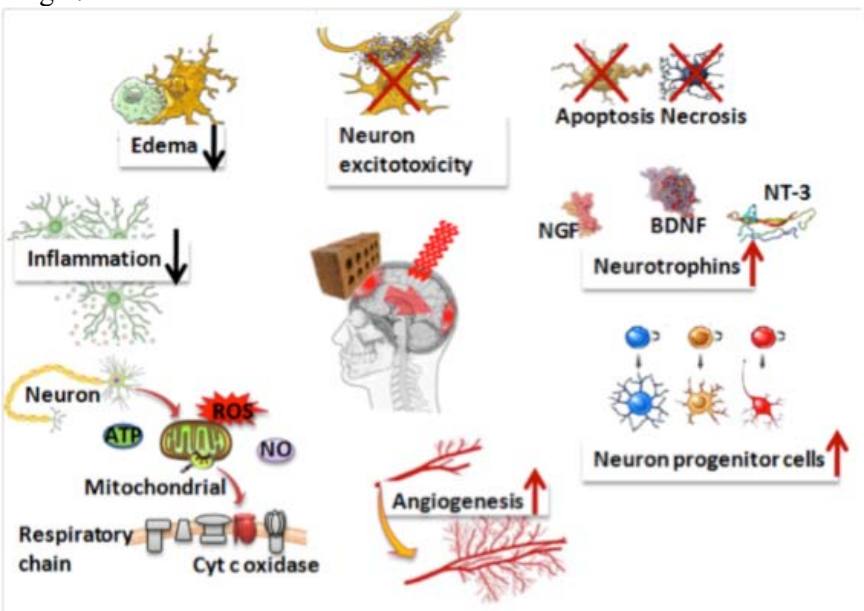

We first tested LLLT in a mouse model of TBI that mimics an impact-acceleration injury similar to that suffered by soldiers who have suffered blast injuries caused by improvised explosive devices. In the closed head impact model the scalp is opened and a weight dropped onto the exposed skull followed by closure of the scalp. In this study we tested 4 different laser wavelengths using exactly the same laser parameters in each case (spot-size of 1 cm^2, fluence of 36 J/cm^2 and irradiance of 150 mW/cm^2). A single laser exposure lasting 4 minutes was delivered 4 hours after the TBI. The data presented in Fig 2A show that beginning on day 5 for 810-nm laser and day 9 for 665-nm laser there was a significant difference in the neurological severity score (NSS) of the LLLT group compared to

control and the improvement became relatively larger and more significant as time progressed. Although there was a trend towards improvement at middle time points with the 980-nm laser it never became significant and in the case of 730-nm laser there was no improvement at all [8].

We next moved to another mouse model of TBI known as the controlled cortical impact (CCI) model. This involves opening the scalp and using a trephine to create a craniotomy (removal of a piece of skull) to expose the dura. A hydraulic piston was then used to make an impact on the exposed brain and form a controlled lesion in the cortex. Laser (of the best wavelength previously determined, 810-nm) was then applied to the head of the mouse 4 hours after the injury. We reduced the dosage to 18 J/cm^2 delivered at 50 mW/cm^2 taking 6 minutes compared to that used in the previous study as evidence suggested that lower doses of light are better than high doses. In one group of mice we delivered the laser treatment once a day for 14 days. Fig 2C shows that the single LLLT treatment had a significant effect of the NSS score commencing at 3 days post-injury. As expected the daily repeated laser treatment also produced an improvement until day 5. Then the improvement ceased for some time and then resumed at the same rate as no treatment control TBI mice. This represents another instance of the biphasic dose response in LLLT. Figure 2C shows that in mice sacrificed at 28 days post-injury that the size of the brain lesion was significantly smaller in the mice that received a single laser treatment. Fig. 2D shows that in brain sections taken at 28 days there is some evidence that the laser treated mice has a greater amount of neurogenesis (new brain cell formation) as revealed by BrdU staining compared to the nor treatment controls. Induction of neurogenesis by transcranial laser may explain many of its beneficial effects in multiple diseases and conditions.

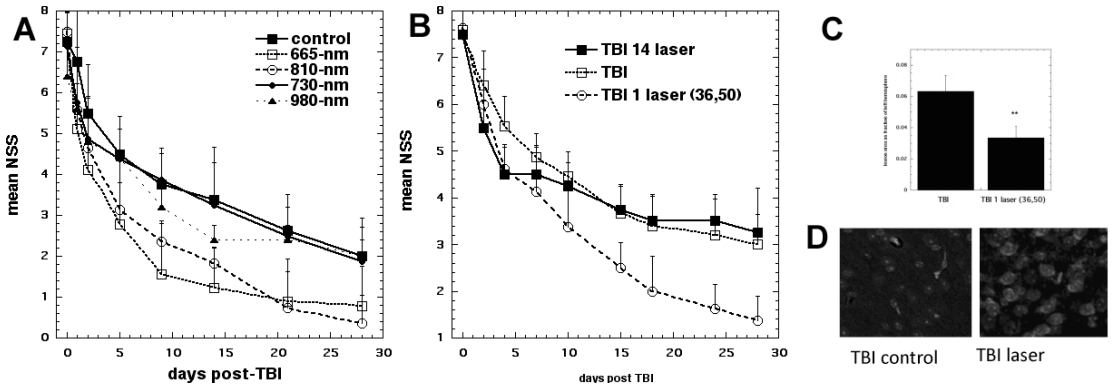

The remarkable effects of LLLT in remedying CNS damage in a non-invasive manner with little evidence of any adverse side-effects, suggest that its application will only increase. Advances that are being made in understanding the molecular and cellular basis for the action of red and near-infrared light on cells and tissues, will only serve to increase the acceptance of LLLT by the medical profession at large. If LLLT can make even a small contribution to mitigating the loss of life, suffering, disability and financial burden caused by CNS disorders, it will make the efforts of researchers in the LLLT field worthwhile.

References

1. R.K. Narayan, M.E. Michel, B. Ansell, *et al.,* "Clinical trials in head injury", *J. Neurotrauma,* 2002, **19,** 503-557.
2. J.S. Jennings, A.M. Gerber, & M.L. Vallano, "Pharmacological strategies for neuroprotection in traumatic brain injury", *Mini Rev Med Chem.,* 2008, **8,** 689-701.
3. K.R. Diller, & L. Zhu, "Hypothermia therapy for brain injury", *Annu Rev. Biomed. Eng.,* 2009, **11,** 135-162.
4. U. Oron, T. Yaakobi, A. Oron, *et al.,* "Low-energy laser irradiation reduces formation of scar tissue after myocardial infarction in rats and dogs", *Circulation,* 2001, **103,** 296-301.
5. Y. Lampl, "Laser treatment for stroke", *Expert Rev. Neurother.,* 2007, **7,** 961-965.
6. X. Wu, A.E. Dmitriev, M.J. Cardoso, *et al.,* "810 nm Wavelength light: an effective therapy for transected or contused rat spinal cord", *Lasers Surg. Med.,* 2009, **41,** 36-41.
7. J.T. Hashmi, Y.-Y. Huang, B.Z. Osmani, *et al.,* "Role of Low-Level Laser Therapy in Neurorehabilitation", *PM&R,* 2010, **2,** S292-S305.
8. Q. Wu, Y.-Y. Huang, S. Dhital, *et al.,* "Low level laser therapy for traumatic brain injury", *Proc. SPIE,* 2010, **7552,** 755206-755201.

ORAL MUCOSA REGENERATION AFTER LASER PATTERNED MICROCOAGULATION TREATMENT: AN ANIMAL STUDY

M. Karabut[1,2], **N. Gladkova**[2], **F. Feldchtein**[3], **Y. Fomina**[4], **E. Kiseleva**[2], **O. Evdokimova**[2], **L. Snopova**[2]

[1] Nizhny Novgorod Lobachevsky State University, Nizhny Novgorod, Russia, maria.karabut@gmail.com
[2] Institute of Applied and Fundamental Medicine, Nizhny Novgorod State Medical Academy Nizhny Novgorod, Russia
[3] Dental Photonics Inc., MA, USA, 02062
[4] Nizhny Novgorod State Medical Academy

Periodontal soft tissue regeneration is important in periodontal therapy. Laser Patterned Microcoagulation (LPM) concept treatment is similar to the use of fractional photothermolysis [1], which has been successfully applied in dermatology [1, 2] and ophthalmology. However, this type of laser treatment has not been applied to oral soft tissues. Oral tissues are known to have even greater regeneration potential than skin [3] because of higher vascularization and faster metabolism. Thus, they are supposed to experience fast scar-free regeneration.

So, the study was designed to perform a feasibility assessment and histological observation of a laser damage formation and regeneration process in the gingival and oral mucosa using an animal model. The second objective of the study was to assess the possibility of cross-polarization optical coherence tomography (CP OCT) for in vivo observation of damage and healing processes of oral soft tissues after LPM. This high-resolution imaging technique is noninvasive and may provide important clinical information for studying the healing dynamics of oral tissues after laser treatment. The technique gives more details about microstructural and biochemical alterations in depolarizing tissue components (collagen).

Eighteen healthy rabbits underwent a single laser treatment *in vivo* in the gingiva and oral mucosa of the rabbit's maxilla at different time points. The rabbits were followed for up to 90 days. There was used a diode laser operating at 980 nm wavelength and generating up to 20 W of power. Each single column was created by a contact application of a tip 400 μm in diameter (Fig. 1) and irradiating the tissue through the tip with a single pulse with duration from 80, 120 and 150 ms. The specimens were stained by hematoxylin and eosin (H&E), picrosirius red (PSR) and nitro-blue-tetrazolium-chloride (NBTC). The NBTC stain revealed a loss of viability in the epithelium and the submucosa after LPM and visualized the broadest area of thermal damage in the column associated with inhibition of oxidative enzymatic activity, with high contrast, which allows laser column size measurement with high accuracy. The column width varied from 0.4 to 0.7 mm, and depth from 1.1 to 1.8 mm at all exposure times (Fig. 2). The column size grew with increasing laser pulse duration.

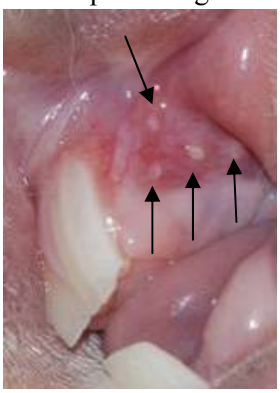

Fig. 1. View of laser columns on rabbit maxilla

a b c

Fig. 2. Laser column 1 hour after laser irradiation: 80 ms – 0.4 x 1.1 mm (a), 120 ms – 0.5 x 1.3 mm (b), 150 ms – 0.7 x 1.8 mm (c). Image size – 0.95 x 0.98 mm

Wound healing is known to run in successive and overlapping stages: inflammation, proliferation, and regeneration (3). Histological analysis of the laser injury zones at 80-150 ms exposure revealed

that in one-two days after LPM the continuity of the epithelial basal cell layer had been restored. Complete epithelial regeneration was obtained within 7-12 days after the treatment (Fig. 3, d, e, f). One day after the treatment a pronounced reactive inflammation developed in the column area. On the 12th day a new collagen was formed at all levels of structural organization, but without horizontal arrangement in the subepithelial layer (Fig. 3, d, e, f). It was confirmed by its polarization properties (Fig. 3, e). By the 90th day, the tissue structure had been completely restored indicating complete healing (Fig. 3, g, h, i).

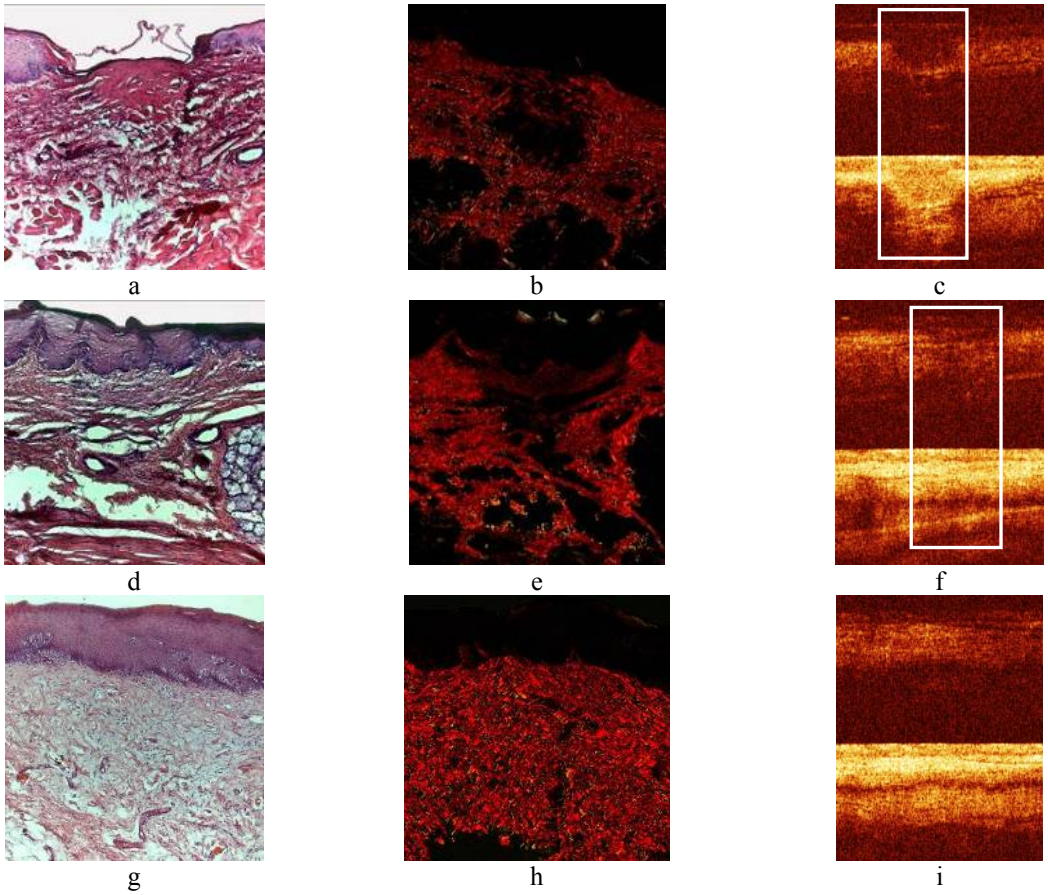

Fig. 3. Laser column healing: a, b, c – inflammation stage; d, e, f – proliferative stage; g, h, i – regeneration stage. HE (a, d, g), PSR (b, e, h), CP OCT image (c, f, i). Image size – 0.95 x 0.98 mm

A single treatment with laser microcoagulation is supposed to induce a wound healing and regeneration response in oral mucosa, which allows considering LPM as a promising method of treating degenerative diseases of oral soft tissues. Exposure time may vary depending on clinical applications. Duration of healing suggests possible repeated LPM not earlier than in a week. CP OCT reveals the most significant changes of the soft oral tissues by laser deposition of the columns and their healing *in vivo*. So, the further using of CP OCT can be helpful when choosing optimal conditions and procedures of a laser treatment for patients.

Acknowledgements

This work was supported by the Russian Foundation for Basic Research (No. 10-02-01175) and State Contract with Ministry of Education and Science of the Russian Federation (No. 02.740.11.5149, 11.G34.31.0017). The authors are grateful to Dental Photonics, Inc (Walpole, MA, USA) for the support of this work.

References

1. D. Manstein, G.S. Herron, R.K. Sink, et al., *Lasers Surg. Med.,* 2004, **34**(5), 426-438.
2. M.H. Jih and A. Kimyai-Asadi, *Semin. Cutan. Med. Surg.,* 2008, **27**(1), 63-71.
3. A.M. Szpaderska, J.D. Zuckerman, L.A. DiPietro, *J. Dent. Res.,* 2003, **82**(8), 621-626.

NOVEL PEG-ORGANIZED BIOCOMPATIBLE FLUORESCENT NANOPARTICLES DOPED WITH AN YTTERBIUM CYANOPORPHYRAZINE COMPLEX FOR BIOPHOTONIC APPLICATIONS

L.G. Klapshina[1], W.E. Douglas[2], I.S. Grigoryev[1], E.Yu. Ladilina[1], S.A. Lermontova[1], M.V. Shirmanova[3], S.A. Mysyagin[4], I.V. Balalaeva[4], N.Yu. Lekanova[4], and **E.V. Zagaynova[3]**

[1] G.A. Razuvaev Institute of Organometallic Chemistry, Russian Academy of Sciences
Nizhny Novgorod, Russia. E-mail: klarisa@iomc.ras.ru
[2] Labo. CMOS, CNRS UMR 5253, Institut Gerhardt
Université Montpellier II, Montpellier, France
[3] Nizhny Novgorod State Medical Academy, Russia
[4] N.I. Lobachevsky State University, Nizhny Novgorod, Russia

Tetrapyrrolic macrocycles and their metal complexes occupy a central place in bioorganic chemistry since they are used in important biomedical applications, particularly in the fields of neoplastic tissue detection and photodynamic therapy (PDT). Recently we reported the first metal-template assembly of the octacyanoporphyrazine framework from tetracyanoethylene structural units [1]. A series of novel ytterbium octacyano- and tetracyanotetraarylporphyrazine complexes (YbCNPz) showing high light absorption in the wavelength range of 600–680 nm has been prepared usign this new synthetic approach [2]. Because of enhanced biological tissue penetrability at longer wavelengths the reported compounds may be interesting as potential PDT photosensitizers characterized by intense absorption in the red.

The successful realization of the PDT concept is crucially dependent on photosensitizer potency for generating singlet oxygen. However, such photosensitizer potency is not sufficient for effective PDT; the photosensitizer must also be water-soluble and biocompatible, these being essential requirements for materials destined for biomedical use.

Usually, the water solubility properties of tetrapyrrollic macrocycles are modified by varying the peripheral substituents. However, the chemical modification of chromophores is often very labour intensive and, indeed, is not always possible. In addition, that eventually causes undisirable photosensitizer photophysical properties changes. Our efforts to develop short and simple routes to biologically relevant forms of novel tetrapyrrolic photosensitizer without chemical modification gave rise to two one-pot strategies of the preparation of light-emitting water soluble nanoparticles incorporating YbCNPz: (i) encapsulation of YbCNPz into non-toxic biocompatible water soluble polyethylene glycol (PEG) macromolecule aggregates (aqueous red fluorescent suspension RFS 1), and (ii) the preparation of biocompatible water soluble uniform nanoparticles consisting of a PEG core framed with fluorinated hybrid silica nanolayers doped with YbCNPz. (aqueous red fluorescent suspension RFS 2), Scheme and Figs. 1 and 2).

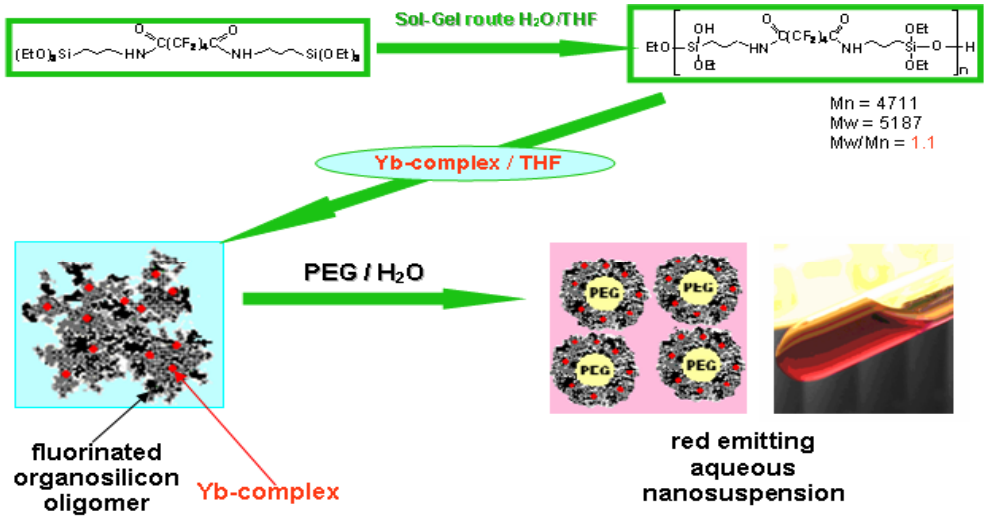

Fig. 1. Preparation of biocompatible PEG-organized water-soluble silica nanoparticles doped with Yb-complex

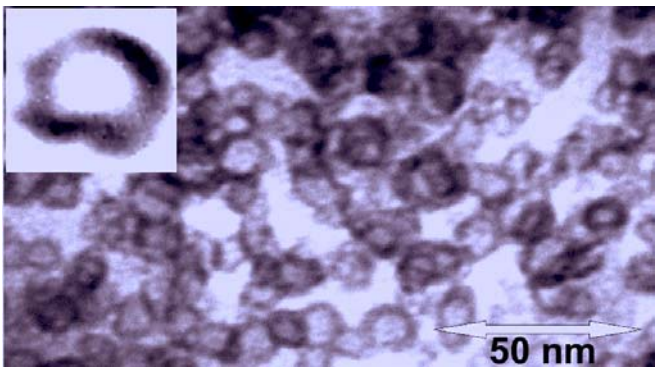

Fig. 2. TEM image of PEG-silica disk-shaped nanoparticles doped with the ytterbium cyanoporphyrazine complex. Insert 3 times magnifide nanoparticle image

A large enhancement of red emission for all the types of nanoparticles is observed in physiological liquids owing to their binding to biomolecules (Table 1).

Table 1. Quantum yield and fluorescence enhancement effect of RFS**1** and RFS**2** in physiological liquids

Quantum yield, ϕ* (Enhancement factor)			
Sample	H_2O	Serum	10 % aqueous albumin solution
RFS**1**	$2.5 \cdot 10^{-3}$	0.10 (50)	0.60(240)
RFS**2**	$5.0 \cdot 10^{-4}$	0.13 (260)	0.19(370)

Thus, effective conjugation of RLS**2** nanoparticles, which are more lipophilic owing to their hydrophobic fluorinated peripheral parts, with the other serum components such as lipoproteins can be assumed. A conjugation with low density lipoproteins (LDL) is of particular interest for PDT in view of the increased level of LDL receptors on cancer cells.

Acknowledgements

Financial support was received from the Russian Basic Research Foundation, the Russian Agency for Education, and the CNRS.

References

1. L.G. Klapshina, I.S. Grigoryev, W.E. Douglas, *et al.*, *Chem. Commun.*, 2007, **43**, 1942-1944.
2. L.G. Klapshina, W.E. Douglas, I.S. Grigoryev *et al*., *J. Mater. Chem*., 2009, **19**, 3668-3676.
3. L.G. Klapshina, W.E. Douglas, I.S. Grigoryev, E.Yu. Ladilina, *et al., Chem. Comm.,* 2010, **46**, 8398-8400.

PROJECT OF 200 J 20 ns 1 SHOT/MINUTE ND:GLASS LASER FOR CPA IN TI:SAPPHIRE

A.A. Kuzmin, A.A. Shaykin, and **E.A. Khazanov**

Institute of Applied Physics of the Russian Academy of Sciences, Nizhny Novgorod, Russia
alexeyhsgap@yandex.ru

Recently an interest in nanosecond Nd:glass lasers has increased all over the world. Such lasers are widely used for experiments on laser thermonuclear synthesis and in other fundamental and applied researches. Nd:glass is indispensable for creation of powerful femtosecond laser setups of petawatt level. These setups have many applications in physics (i.e. electron and ion acceleration) and in medicine (i.e. tomography and hadronic therapy).

In all types of petawatt lasers and projects energy is initially reserved in a nanosecond pulse of Nd:glass laser. Limitations on pulse repetition rate are thermal effects in Nd:glass caused by low heat conductivity and large aperture of glass amplifiers. A basic restriction is glass fracture when the thermally induced pressure threshold is exceeded. In practice, however, lasers work with smaller repetition rates because of accumulation of radiation depolarization and strong aberrational thermal lens. All these effects reduce the quality of laser radiation.

A typical repetition rate of available petawatt lasers is 1 shot per 30 minutes or less. An increase of repetition rate is an urgent problem, because it simplifies solutions of applied tasks decreasing the value of the pulse.

We have analyzed thermally induced effects in Nd:glass rods 4.5, 6, 8.5 and 10 cm in aperture at a pulse repetition period of about a minute. The analysis showed that active elements 4.5 cm in diameter can produce up to 110 J of energy in 20 ns pulses (λ = 1054 μm) operating once a minute and having a safety factor of at least 5 before damage. Using the larger rods in such a regime is risky. The results of studies of thermally induced depolarization (Fig. 1) and thermal lens in a 4.5 cm in aperture Nd:glass rod amplifier are reported in this paper.

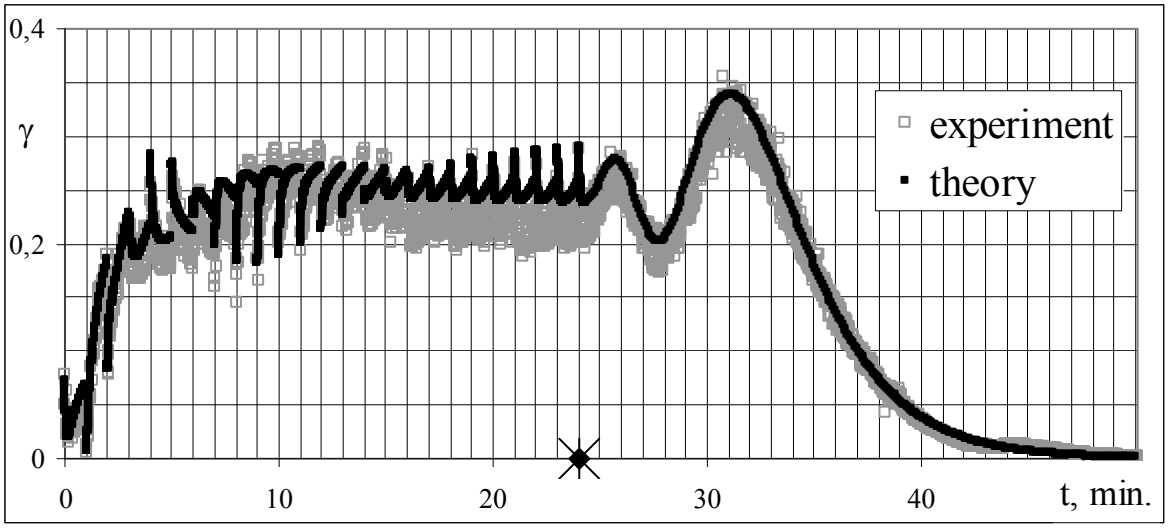

Fig. 1. Polarization loses γ in Nd:glass rod with the aperture of 4.5 cm in the run of pump pulses followed one by one with a period of 1 minute. The asterisks designate the last pump pulse in the run

Our investigation shows the possibility of creating a 340 J 20 ns (λ = 1054 μm) Nd:glass laser with pulse repetition period of about a minute (Fig. 2). After frequency doubling (type 2 phase matching) we expect up to 200 J of energy at λ = 527 μm. This radiation can be used as a pump for a Ti:Sa crystal. It allows generating sub-petawatt pulses with record repetition rate. Strong phase and polarization distortions need to be compensated. Results of the corresponding experiments are reported as well (Fig. 3).

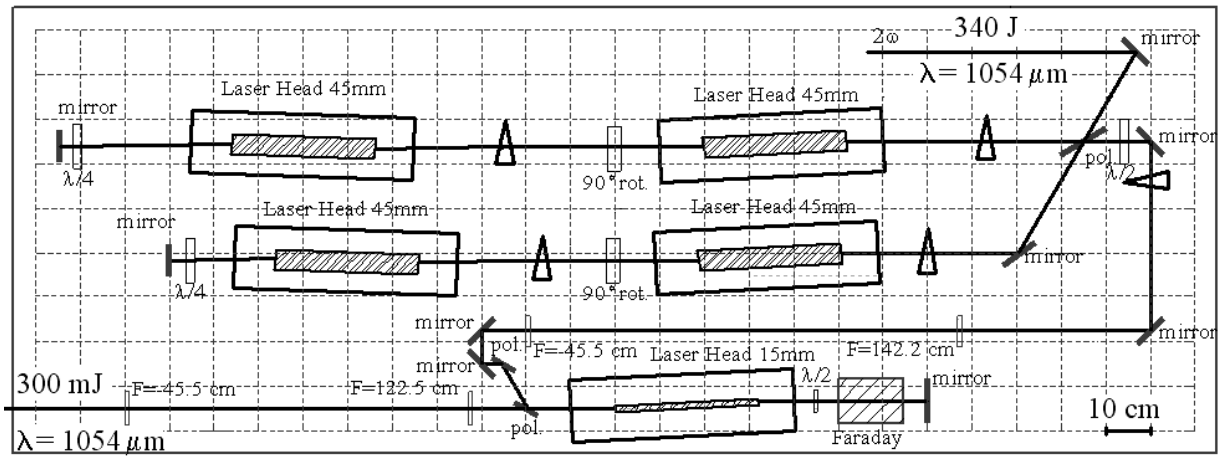

Fig. 2. A principal scheme of 340 J 20 ns (λ = 1054 μm) Nd:glass laser with repetition rate 1 pulse per 1 minute

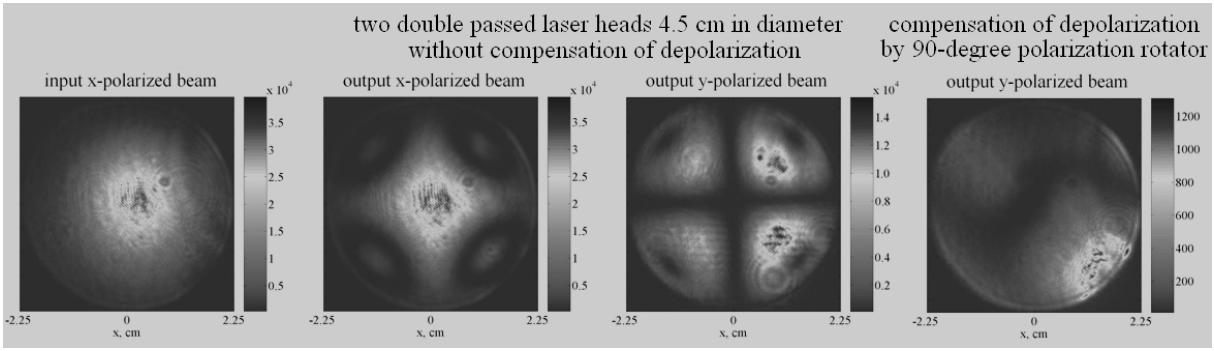

Fig. 3. Compensation of depolarization in two double passed Nd:glass rods 4.5 cm in diameter by a crystalline 90-degree polarization rotator (W_{pump} = 29.2 kJ, pump pulse repetition period is 3 minutes)

Acknowledgments

This work was supported by the program of the Presidium of the Russian Academy of Sciences "Extreme Light Fields: Sources and Applications".

THEORETICAL AND EXPERIMENTAL INVESTIGATION THE CUBIC NONLINEARITY AND THERMALLY INDUCED BIREFRINGENCE INFLUENCE ON CONTEMPORARY PW LASER SYSTEMS

M.S. Kuzmina, M.A. Martyanov, A.K. Poteomkin, E.A. Khazanov, and **A.A. Shaykin**

Institute of Applied Physics RAS, Nizhny Novgorod, 46 Ulyanov Street, 603950, Russia,
kmsnn@mail.ru

The state-of-the-art powerful laser systems may be conventionally divided into two classes: high peak power and high average power lasers. Parasitic effects that are due to cubic nonlinearity in the first case and to thermally induced birefringence in the second case are imposed on operation of both laser types.

The negative consequence of depolarization is that after passage through the polarizer, the polarized radiation is amplitude and phase modulated (e.g., cross wheel and astigmatism, respectively). This reduces the power in the initial single-mode beam due to polarization amplitude and phase distortions.

Media with cubic nonlinearity are characterized by the dependence of refractive index on intensity $n(I) = n_0 + \gamma_{NL} I$, where n_0 is the linear index of refraction, γ_{NL} is the characteristic of a nonlinear medium, and I is radiation intensity. B-integral, i.e., the nonlinear phase incursion in a medium with length L, is taken as a measure of nonlinearity: $B = \frac{2\pi}{\lambda}\gamma_{NL}\int_0^L I(z)dz$, where λ is the wavelength of light in vacuum, and r is the radius in the cylindrical reference frame. Anisotropy appears in a medium with cubic nonlinearity. The arising difference in the refractive indices of circularly polarized components of radiation leads to the phase difference between them and, as a consequence, to rotation of the polarization ellipse. Thus, both cubic nonlinearity and thermally induced birefringence introduce polarization distortions in the laser beam, giving rise to depolarization, the contributions of both the effects being nonadditive.

Rapid advance of laser technologies facilitates creation of lasers combining the features of available high average and high peak power lasers. Apparently, when developing such lasers one should take into account joint parasitic influence of cubic nonlinearity and thermally induced birefringence on the quality of laser radiation. No such studies have been undertaken before. Another challenging problem is mutual action of the above effects on efficiency of the broadly employed methods of minimization and compensation of each effect separately. The following results were obtained in the current paper.

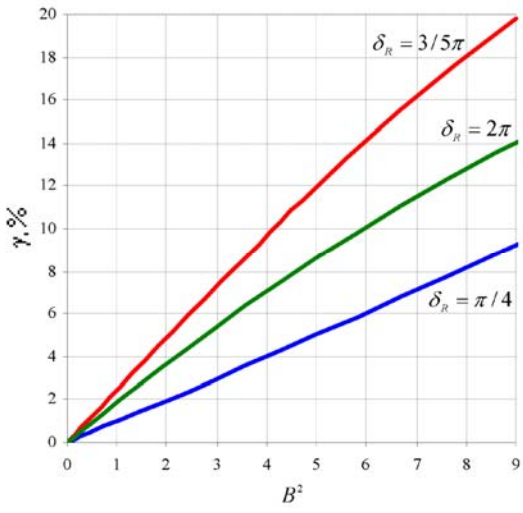

Fig. 1. Function $\gamma(B^2)$ at the output of the depolarization compensation system for initial linear polarization

A system of differential equations describing laser radiation propagation in a medium with cubic nonlinearity in the presence of birefringence was derived [2]. It was shown that the efficiency of compensation of thermally induced polarization in two identical birefringent nonlinear elements (NE) by means of 90° polarization rotator placed between them decreases with increasing B-integral. The magnitude of uncompensated depolarization in such a scheme is proportional to B^2 to a high accuracy (fig. 1) for arbitrary values of thermally induced phase difference δ at the periphery of the beam. Hereinafter all parameters (B, δ) correspond to one medium.

For a circular incident polarization, the angle of polarization rotation χ, in terms of better depolarization compensation, should not be equal to 90°. The values of optimal rotator angles χ_{opt} ensuring residual depolarization of about 1% were found numerically for different magnitudes of thermally induced birefringence. The presented analysis of the

joint influence of cubic nonlinearity and thermally induced birefringence was done neglecting amplification in nonlinear elements.

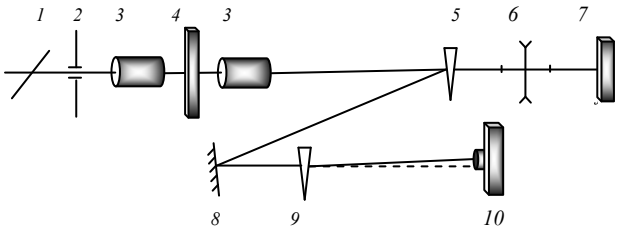

Fig. 2. Experimental scheme: *1* – polarizer, *2* – aperture diaphragm Ø2 mm, *3* – NE Ø100 mm, 4 – 90° polarization rotator, 5 – glass wedge, 6 – lens, 7 – pirodetector Gentec QE50, 8 – mirror, 9 – calcite wedge, 10 – CCD camera and filters. Dash line corresponds to depolarized component of radiation

The increase of residual depolarization degree with *B*-integral growth in the scheme of depolarization compensation with the help of 90º polarization rotator was confirmed experimentally (fig. 2). The birefringence was induced in NEs by the single flash from the pump lamps, arranged along the generating line of the NE. Laser beam (2 mm in diameter) passed through two NE (Nd:glass rods 100 mm in diameter) and 90º polarization rotator and partly reflected from the glass wedge and, then, propagated through the calcite wedge. Finally, the images of radiation components with initial linear polarization and orthogonal polarization were both projected to the same CCD-camera. The software processing of obtained transverse distributions of these components allowed us measuring the local degree of depolarization *Γ*. The energy of the pulse was measured by pirodetector 7. In experiments we used 20 ns and 1 ns pulses with energies in the range of 10 mJ – 2 J coming from subpetawatt "PEARL" start-up laser setup [3].

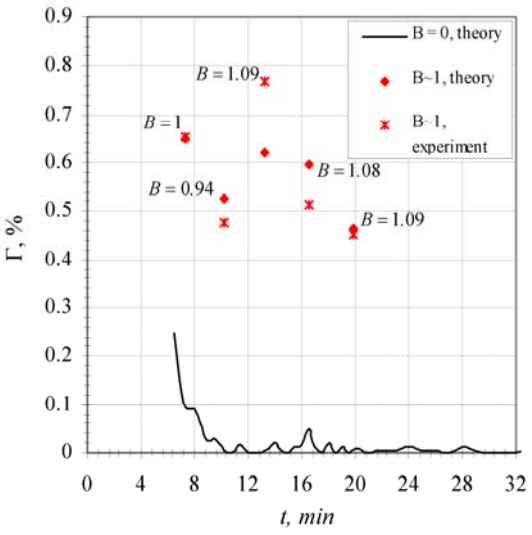

Fig. 3. Theoretical and experimental function *Γ*(*t*) at the output of the scheme on fig. when $B = 0$ and $B \sim 1$

In the first two series the time dependence of the local depolarization degree was obtained separately in first and second NE when *B*-integral was equal to zero. This determinates identity of NEs used in the experimental scheme (fig. 2) and, consequently, the amount of the residual depolarization degree in the scheme of depolarization compensation when *B*-integral is equal to zero.

In the third series local depolarization degree *Γ* was measured at the output of the scheme fig. 2 for various values of *B*-integral. The results of this experiment are depicted in fig. 3. One can easily see that then *B*-integral is equal to zero the residual local depolarization degree doesn't exceed 0.1%. Contrary to this case, when *B*-integral is about unity in each NE the residual depolarization increases up to 0.7%.

Notice, the experimental and theoretical results are in the good agreement. Therefore, we can conclude that system of equations correctly describes the laser radiation propagation in the medium with cubic nonlinearity and thermally induced birefringence.

References

1. A.K. Poteomkin, et. al., "Compact 300 J/ 300 GW frequency doubled neodimium glass laser. Part I: Limiting power by self-focusing", *IEEE JQE*, 2009, **45**, 336-344.
2. M.S. Kochetkova, et. al., "Propagation of laser radiation in a medium with thermally induced birefringence and cubic nonlinearity", *Opt. Exp*., 2010, **18**, 12839-12851.
3. E.A. Khazanov, et. al., "Compact 300 J/ 300 GW frequency doubled neodimium glass laser. Part II: Description of Laser setup", *IEEE JQE*, 2009, **45**, 854-862.

BIOCOMPATIBLE POLYMERIC NANOPARTICLES DOPED WITH YTTERBIUM PORPHYRAZINE AS POTENTIAL PHOTOSENSITIZER

N.Y. Lekanova[1], **M.V. Shirmanova**[2], **I.V. Balalaeva**[1], **L.G. Klapshina**[3], and **E.V. Zagaynova**[2]

[1] N.I. Lobachevsky State University of Nizhny Novgorod, Russia
nat-lekanova@yandex.ru
[2] Nizhny Novgorod State Medical Academy, Russia
[3] Nizhny Novgorod Institute of Organometallic Chemistry RAS, Russia

Photodynamic therapy (PDT) is based on photosensitizers (PSs) selectively accumulating in pathological tissues and producing cytotoxic singlet oxygen under irradiation. No ideal PS which would meet all the clinical requirements has been found so far, therefore development of novel PSs is still topical. The purpose of our study was to test the functional properties of a potential photosensitizer based on biocompatible polymeric nanoparticles dopped with ytterbium tetracyanotetraphenylporphyrazine (YPz).

Materials and methods

Ytterbium tetracyanotetraphenylporphyrazine (Fig. 1) was synthesized and converted into stable biocompatible water-soluble forms by forming polymeric nanoparticles [1].

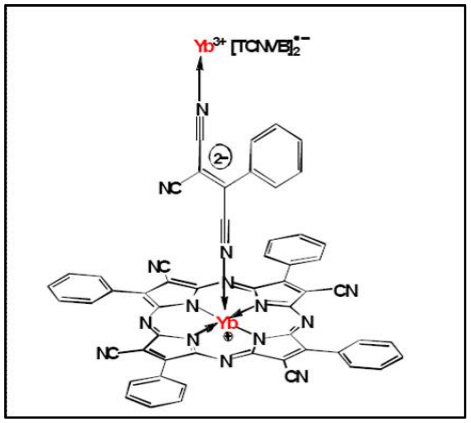

Fig. 1. Tetracyanotetraphenylporphyrzine ytterbium complex

Absorption and fluorescence spectra have been obtained for nanoparticles of different composition and fluorescence intensity dependence on polymer type and medium characteristics (water, blood serum, albumin solution) has been investigated. Ytterbium porphyrazine was also tested as the singlet oxygen producer. For $^1O_2$ registration we used its ability to phosphoresce at 1270 nm.

For *in vitro* research of cellular uptake of the YPz nanoparticles we used SKBR-3 cell line (human breast carcinoma). Cells were incubated with YPz (40 mkg/ml) for 30 minutes. Intracellular localization of the YPz was studied by confocal laser scanning microscopy.

A whole-body imaging experiment was carried out using a fluorescence transilluminative imaging setup with low-frequency modulation and transilluminative configuration of scanning created at the Institute of Applied Physics RAS (Russia) [2]. In this setup synchronous scanning of the object in the transilluminative configuration is provided by a single pair of a source and a detector set. As a source of excitation light we employed a semiconductor laser at 635 nm. As a detector of fluorescent light we used a high-sensitivity cooled photomultiplier tube Hamamatsu H7422-20. Emission signal was filtered using a 685 to 735 nm band-pass filter. Image acquisition time per animal was 3–5 minutes. Previously, serial imaging of the same animal showed that this technique was capable of estimating photosensitizer accumulation in transplantable tumor and washout over time in individual animals [3]. Quantification of the fluorescence in the tumor area provided an opportunity to determine tumor uptake and retention kinetics.

The experiments were performed on 20 female CBA mice bearing cervical carcinoma. To investigate the YPz pharmacokinetics, the mice were imaged *in vivo* for 15 min and 1, 2, 3, 4, 6, and 24 hrs following the chemicals administration. The image obtained before injection was used as a control one. For verification of photosensitizer accumulation in tumor tissue, fluorescence was analyzed by standard methods — confocal microscopy and fluorescence spectroscopy *ex vivo*.

Results

The synthesized YPz and its biocompatible nanoparticles demonstrated light absorption with maximum at 590 nm and strong fluorescence at around 640 nm. A large enhancement of red emission

of the nanoparticles in serum and albumin was detected. This effect is supposed to result from their bindings to proteins. A possibility of singlet oxygen generation by the YPz nanoparticles was confirmed. The YPz particles with polyethylene glycol (YPz-PEG) were chosen for testing biological properties.

In experiments on cell culture we revealed that the YPz-PEG nanoparticles were internalized and accumulated in the tumor cells around the nucleus. We suppose they are preferably localized in lysosomes. Experiments on mice bearing transplanted cervical carcinoma demonstrated rather suitable pharmacokinetics of the YPz-PEG (Fig. 2). 3 hours after the intravenous injection of the YPz-PEG in 10 mg/kg dose it accumulated in the tumor tissue and retained there up to 6 hours. However, tumor selectivity of the potential photosensitizer was quite low. After 2 days complete elimination of the complex from the animal body was not observed. A prolonged (more than 6 days) retention of the YPz-PEG was typical for the tumor. The kinetics of tumor uptake of the YPz-PEG obtained by transillumination imaging *in vivo* agrees to the data of standard *ex vivo* methods.

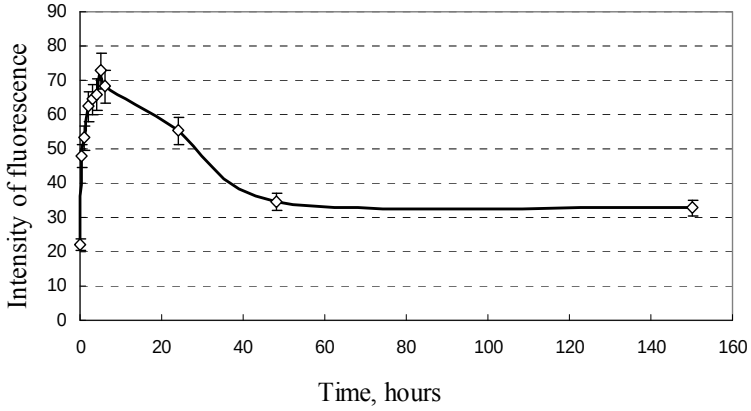

Fig. 2. Kinetics of *in vivo* tumor uptake and washout of YPz-PEG (10 mg/kg)

Conclusions and perspectives

In general, the ytterbium porphyrazine nanoparticles are of interest as photosensitizers for fluorescence diagnostics and/or PDT due to their optical and biomedical characteristics. Hereafter we plan to test other forms of YPz with chemical modifications in porphyrazine structure as well as nanoparticles of different polymer composition in order to select one with absorption and fluorescence at longer wavelengths and selective accumulation in tumor.

Acknowledgements

This work was partly supported by the Ministry of Education and Science of the Russian Federation (project #02.740.11.0086), the Russian Foundation for Basic Research (projects ## 11-04-97100, 10-03-90006), and the Program of RAS Presidium "Fundamental Sciences for Medicine".

References

1. L.G. Klapshina, W.E. Douglas, I.S. Grigoryev et al., *J. Mater. Chem.,* 2010, **46**(44), 8398-8400.
2. I.V. Turchin, V.A. Kamensky, V.I. Plehanov et al., *J. Biomed. Opt*., 2008, **13**(4), 041310.
3. M.V. Shirmanova, E.V. Zagaynova, M.A. Sirotkina et al., *J. Biomed. Opt.,* 2010, **15**(4), 048004.

Invited

DOES PDT HAVE A FUTURE FOR INTRACRANIAL NEOPLASM: ENGINEERING AND BIOLOGICAL APPROACHES TO INCREASE SURVIVAL

L. Lilge[1], **C. Fisher**[2], and **J. Eubanks**[3]

[1] Ontario Cancer Institute and University of Toronto, Canada, Llilge@uhnres.utoronto.ca
[2] University of Toronto, Canada
[3] University Health Network and Institute of Medical Sciences University of Toronto, Canada
llilge@uhnres.utoronto.ca

Despite some success of PDT in the treatment of surfaces of organs, such as skin, oesophagus, bladder and so on, success concerning intracranial neoplasm is still eluding, notwithstanding the considerable progress in fluorescence surgical guidance [1]. Next to variability in photosensitizer distribution due the blood brain barrier and oxygen availability, the tissues inherent responsivity to PDT can further degrade the local selectivity of PDT treatment. The latter is particularly true for ALA-induced PPIX or Photofrin mediated PDT of intracranial neoplasm, which showed that the intrinsic responsivity of normal glial and neuronal cells essentially eliminates the selectivity of neoplastic photosensitizer uptake [2]. Hence, in order to limit neuronal damage and achieving confinement to the neoplastic tissue, PDT delivery needs to consider conformal illumination or reducing the fluence dose at the expense of achieving very high therapeutic tumor resection.

Conformal exposure limits

Within the concept of the PDT threshold model[3] the requirements for conformal therapy can be met through the minimization of

$$F = \sum_{j=1}^{R} w_j^t f(\phi, \phi_T) + \sum_{j=1}^{O} w_j^{OAR} f(\phi, \phi_N), \quad (1)$$

where the first term on the right describes the dose to the tumor, while the second describes the dose to the neurons or organ at risk, and $f(\phi, \phi_T)$ or $f(\phi, \phi_N)$ is < 0, if the actual dose, ϕ, and the tissue threshold dose, $\phi_{T,N}$, relate as $\phi < \phi_T$ in the tumor or $\phi > \phi_N$ for normal neurons, indicating an undesirable dose level and $f > 0$ otherwise. w^t and w^{OAR} are respective weighting factors and can be modified based on the need to destroy or preserve respective tissue voxel j. $\phi_{T,N}$ are the threshold values of tumor and normal tissue and are given by

$$\phi_{T,N} = 2.3 \varepsilon C H(r) \quad (2)$$

with ε being the photosensitizer extinction coefficient, C its concentration and H the fluence at distance r from the source or resection cavity surface. To maximise eq. (1) one needs to satisfy eq. (2) in the following form

$$\frac{C_T H(r)}{\phi_T} \geq \frac{C_N H(r)}{\phi_N}, \quad (3)$$

where the fluence $H(r)$ is given by the tissue optical properties of the normal brain modified by the magnitude of the malignant infiltrate and. hence, conformal fluence rate cannot recuperate the lost selectivity due to the unfavorable $\phi_T > \sim 10 * \phi_N$. So, conformal light irradiation is desirable on an organ level, if particular areas need to be spared or in interstitial application. While no gains in the photosensitizer selectivity can easily be expected, the intrinsic tissue sensitivity to PDT as expressed through their threshold values $\phi_{T,N}$ should be considered.

Use of neuroprotectant in PDT

EPO and IGF-1 co-treatment has been proposed due to their ability to lead to neuroprotection in a variety of treatment modalities both in vitro and *in vivo* [4, 5]. EPO itself has been demonstrated to act as a neuroprotectant following stroke and traumatic brain injury, as well as a variety of insults on cortical neurons in vitro [6, 7]. In addition, EPO has been proposed to act on the PI3K-AKT-mTOR pathway and furthermore leading to neuroprotection. Furthermore, IGF-1 has also been deemed a

potent activator of AKT, and co-treatment of EPO/IGF-1 has been proposed to lead to greater activation of AKT than either treatment alone [4]. Alternatively, Colbourne et al. [8] have examined the effects of mild hypothermia (32-34 degrees Celsius) following traumatic brain injury, stroke, and arterial occlusion [8, 9] and all groups reported significant increased neuronal function following treatment, although the exact mechanism is not known.

The potential of this neuroprotective approach was demonstrated through qRT-PCR performed on rat cell lines and comparing the EPOR expression between PC12 (a neuronal-like cell line), dPC12 (NGF differentiated PC12 cells – mimic a sympathetic neuron) and 9L and F98 (rat glioma cell lines). Results showed indeed, as reported in the literature, that PC12 and dPC12 cells had the highest amount EPOR mRNA, compared to the two glioma cell lines. Similar result was shown in some human cell lines. The cell lines were U87MG (a human Grade IV GBM cell line), SH-SY5Y (a neuronal-like cell line), and K562 (a human CML cell line which has EPOR on its surface).

Treatment of IGF-1and EPO, in our neuronal-like PC12 cell lines, as well as primary neural tissue and our glioma cell line resulted in large amounts of phosphorylation of AKT above baseline in both primary cortical neurons and differentiated PC12 cells but no increase in phosphorylation of AKT in our human glioma cell line. Moreover, co-treatment did induce a larger amount of pAKT, at lower drug concentrations and IGF-1/EPO co-treatment led to phosphorylation of AKT for hours following treatment in differentiated PC12 cells providing ample time for treatment prior to PDT and the immediate post PDT inflammatory phase.

Further in vitro experiments showing the gain in ϕ_N for ALA mediated PDT are ongoing and first results will be presented at the conference.

Hypothermia was induced 1 hour prior to PDT light treatment and 2 hours following light exposure at 32 ºC. Brains were extracted 24 hours later and subjected to H&E and Fluorojade-C staining. Hypothermic PDT animals showed less neuronal cell death, across the pial brain surface and in the hippocampus compared to normothermic controls, albeit a full statistical analysis is still pending, so will be available for the conference.

In summary, while it is still uncertain if these neuroprotective pathways are sufficient to revert the unfavorable PDT threshold values of $\phi_T > \sim 10 * \phi_N$ to equality or even revert them, a factor of 3 change is essentially providing selectivity over one light penetration depth and in the case of 635 nm light this equates to a depth selective improvement over 2.4 mm. As over 80% of all recurrences are within 20 mm of the resection cavity each factor of 3 increase in ϕ_N can have significant improvement in patient survival. Additionally, combination of IGF-1/EPO and hypothermia need to be evaluated.

Acknowledgements

The work was funded in part through a grant by the Canadian Institute of Health Research and the Ontario Ministry of Health and Long-term Care.

References

1. W. Stummer, et al., *Neurosurgery,* 2008, **62**, 564-576.
2. L. Lilge, B.C. Wilson, *Journal of Clinical Laser Medicine & Surgery*, 1998, **16**, 81-91. doi:10.1089/clm.1998.16.81.
3. M.S. Patterson, B.C. Wilson, R. Graff, *Photochemistry and Photobiology*, 1990, **51**, 343–349. doi: 10.1111/j.1751-1097.1990.
4. M. Digicaylioglu, G. Garden, S. Timberlake, L. Fletcher, and SA Lipton, *PNAS,* 2004, **101**, 9855-9860.
5. Y.J. Kang, et al., *Annals of Neurology,* 2010, **68**, 342-352.
6. T. Yamashita, N. Nonoguchi, T. Ikemoto, SI. Miyatake, and T Kuroiwa, *Neurological Research,* 2010, 1-6.
7. M. Um, A.W. Gross, and H.F. Lodish, *Cellular Signalling,* 2007, **19**, 634-645.
8. B. Florian, et al., *Neuroscience Letters,* 2008, **438**, 180-185.
9. D.L. Clark, M. Penner, S. Wowk, I. Orellana-Jordan, and F. Coulborne, *Experimental Neurology,* 2009, **220**, 391-399.

Invited

NEW COHERENT X-RAY SOURCE BASED ON RELATIVISTIC HIGH HARMONIC GENERATION IN GAS JET TARGETS

A. S. Pirozhkov[1], M. Kando[1], T. Zh. Esirkepov[1], P. Gallegos[2,3], H. Ahmed[4], E. N. Ragozin[5,6], A. Ya. Faenov[1,7], T. A. Pikuz[1,7], T. Kawachi[1], A. Sagisaka[1], J. K. Koga[1], M. Coury[3], J. Green[2], P. Foster[2], C. Brenner[2,3], B. Dromey[4], D. R. Symes[2], M. Mori[1], K. Kawase[1], T. Kameshima[1], Y. Fukuda[1], L. M. Chen[1,8], I. Daito[1], K. Ogura[1], Y. Hayashi[1], H. Kotaki[1], H. Kiriyama[1], H. Okada[1], N. Nishimori[9], T. Imazono,[1] K. Kondo[1], T. Kimura[1], T. Tajima[1,10], H. Daido[1], P. Rajeev[2], P. Mckenna[3], M. Borghesi[4], D. Neely[2,3], Y. Kato[1,11], and **S. V. Bulanov[1,12]**

[1]Advanced Beam Technology Division, Japan Atomic Energy Agency, Kizugawa, Kyoto, Japan
pirozhkov.alexander@jaea.go.jp
[2]Central Laser Facility, Rutherford Appleton Laboratory, STFC, Didcot, United Kingdom
[3]Department of Physics, SUPA, University of Strathclyde, Glasgow, United Kingdom
[4]School of Mathematics and Physics, Queen's University Belfast, Belfast, United Kingdom
[5]P. N. Lebedev Physical Institute of the Russian Academy of Sciences, Moscow, Russia
[6]Moscow Institute of Physics and Technology (State University), Dolgoprudnyi, Russia
[7]Joint Institute for High Temperatures, Russian Academy of Sciences, Moscow, Russia
[8]Institute of Physics of the Chinese Academy of Sciences, Beijing, China
[9]Laser Application Technology Division, Japan Atomic Energy Agency, Tokai, Ibaraki, Japan
[10]Ludwig-Maximilians-University Munich, Munich, Germany
[11]The Graduate School for the Creation of New Photonics Industries, Hamamatsu, Shizuoka, Japan
[12]A. M. Prokhorov Institute of General Physics, Russian Academy of Sciences, Moscow, Russia

Experimental results

We experimentally demonstrate new regime of high-order harmonic generation by relativistic-irradiance lasers in gas jet targets [1]. The experiments were performed with 9 TW J-KAREN laser (JAEA, Japan) [2] and 120 TW Astra Gemini laser (CLF RAL, UK) [3]. Bright harmonics with both the odd and even orders are emitted in the forward direction, while the base harmonic frequency is downshifted. The harmonics are generated by linearly as well as circularly polarized pulses. Typical examples of obtained spectra are shown in Figs. 1 and 2.

With the 9 TW laser, the harmonics extend to the spectrograph throughput cutoff at 360 eV, which is within the 'water window' spectral region. The harmonic energy within the 'water window' is 0.8±0.1 μJ/sr. With the 120 TW laser producing ~40 μJ/sr per harmonic at 120 eV we demonstrated the scalability of harmonic generation process in terms of photon number.

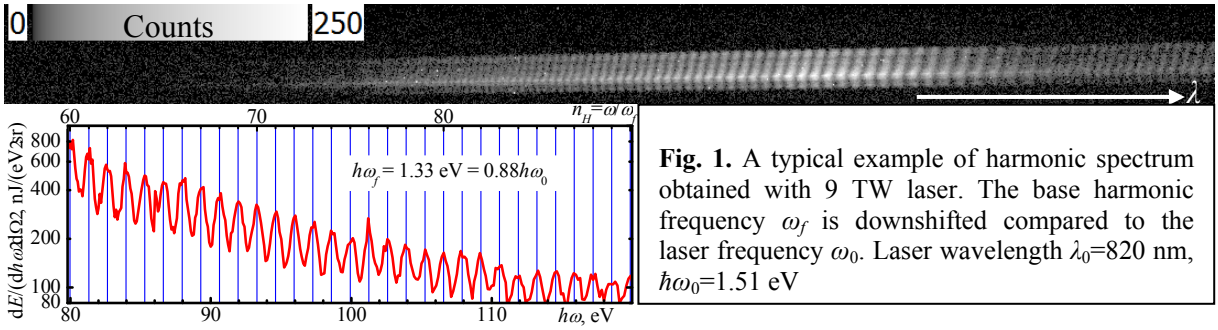

Fig. 1. A typical example of harmonic spectrum obtained with 9 TW laser. The base harmonic frequency ω_f is downshifted compared to the laser frequency ω_0. Laser wavelength λ_0=820 nm, $\hbar\omega_0$=1.51 eV

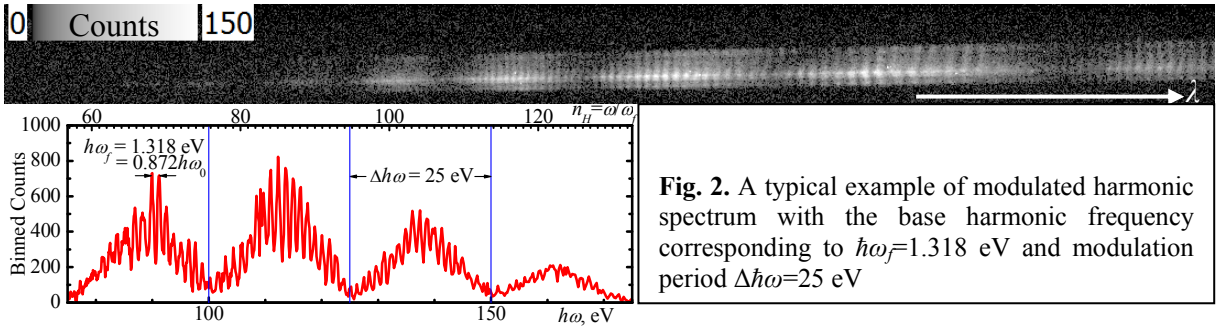

Fig. 2. A typical example of modulated harmonic spectrum with the base harmonic frequency corresponding to $\hbar\omega_f$=1.318 eV and modulation period $\Delta\hbar\omega$=25 eV

New harmonic generation mechanism

The experimentally demonstrated harmonics cannot be explained by previously suggested scenarios, e.g. atomic harmonics, betatron radiation, or nonlinear Thomson scattering. Based on high-resolution 2D and 3D PIC simulations, we introduce a novel mechanism of high-order harmonic generation by relativistic-irradiance lasers in underdense plasmas [1]. The mechanism is based on the phenomena inherent in the relativistic laser–plasma interactions, namely self-focusing [4, 5], cavity evacuation [5, 6], and bow wave generation [7], and collective radiation of an electron density spike driven by electromagnetic field [8]. The formation of density spike with sufficiently small size and large electron number is explained with mathematical catastrophe theory [9]. The cavity and bow wave generation results in the formation of two 'fold'-type singularities in the electron density distribution corresponding to the cavity wall and bow wave front. At the joining of these two singularities, a higher-order 'cusp' singularity is formed. This cusp, or electron density spike, oscillates in the field of self-focused laser pulse, which leads to the collective radiation of high-order harmonics.

Possible applications

The high order harmonics produced by relativistic laser in gas jet represent a new class of compact sources of ultrashort coherent XUV and X-ray pulses. Such source is realizable with a university-laboratory scale laser and a gas jet target which is debris-free, self-replenishable, and suitable for repetitive operation. The source can be used for the femtosecond or attosecond imaging, including possibility of ultrafast high-contrast imaging of biological and medical samples in the 'water window' spectral region. The conservatively estimated peak brightness, e.g. $\sim 10^{23}$ photons/(mm^2 mrad^2 s 0.1% bandwidth) at 120 eV, approaches values characteristic for the 3rd generation synchrotrons. This may lead to the possibility of diffractive x-ray imaging. As an additional benefit, high-order harmonic radiation properties can provide important information about the processes in the relativistic laser plasma, which can be used for diagnostics.

Acknowledgements

The work was supported by MEXT (Kakenhi #20244065, 21604008, 21740302, and 23740413), JAEA President Grant, and STFC (facility access funding).

References

1. A.S. Pirozhkov, M. Kando, T. Zh. Esirkepov, *et al*., *arXiv*:1004.4514, 2010.
2. H. Kiriyama *et al*., *Opt. Lett*., 2008, **33**, 645.
3. C.J. Hooker *et al*., *J. de Phys. IV,* 2006, **133**, 673.
4. G.A. Mourou *et al*., *Rev. Mod. Phys*., 2006, **78**, 309.
5. E. Esarey *et al*., *Rev. Mod. Phys*., 2009, **81**, 1229.
6. A. Pukhov and J. Meyer-ter Vehn, *Appl. Phys. B,* 2002, **74**, 355.
7. T.Zh. Esirkepov *et al*., *Phys. Rev. Lett*., 2008, **101**, 265001.
8. L.D. Landau and E.M. Lifshitz, *The classical theory of fields*, 4th revised English edition (Butterworth-Heinemann, 2003).
9. T. Poston and I. Stewart, *Catastrophe theory and its applications* (Dover, 1996).

LASER TREATMENT OF PLASMA-SPRAYED HYDROXYAPATITE COATINGS OF DENTAL IMPLANTS

I.A. Popov, V.A. Papshev, E.L. Surmenko, and **T.N. Sokolova**

Saratov State Technical University, Russia, e-mail:antaresrock@yandex.ru

The paper describes a method of improving the biological properties of plasma-sprayed bioceramic coatings by IR pulsed laser (Nd:YAG).

Laser treatment is a topical direction of modification of structural-phase state of substances [1-3]. At present progress in the field of dental implantology involves application of new biocomposite materials with improved properties of biocompatibility and mechanical strength. An example is the dental implant with a bioactive coating based on tricalcium phosphate (TCP), hydroxyapatite (HA), etc. The basis of such implants is made of bio-inert and mechanically strong metal (Ti, Zr, Ta). Electro-plasma spraying provides coatings with specified characteristics of porosity and surface roughness, but this leads to undesirable changes in the structural-phase composition, in particular, amorphization [4]. In this paper we consider creation of directed structural phase transformation in the structure of the coating of dental implants by IR laser radiation.

Influence of laser radiation on the structure of coating

When studying the influence of laser radiation on the structure of the coating it is important to choose technological modes to increase the amount of crystalline phase in the coating with a minimum destruction and minimum melting of the surface. Laser radiation well absorbed in the ceramic would be the optimal solution [5]. Pulse YAG laser was taken, because its wavelength 1.06 μm falls on the band of fundamental absorption of the material. Analysis of the experiments shows that results are achieved for laser in a free-running mode with a power density q=(2-6)×10^4 W/cm^2, pulse duration τ=4 ms, pulse repetition rate f=4-15 Hz. Modes were selected using optical microscopy (Fig. 1). The processing speed of the surface by laser radiation was chosen so that the spots crossed each other in 50-80%.

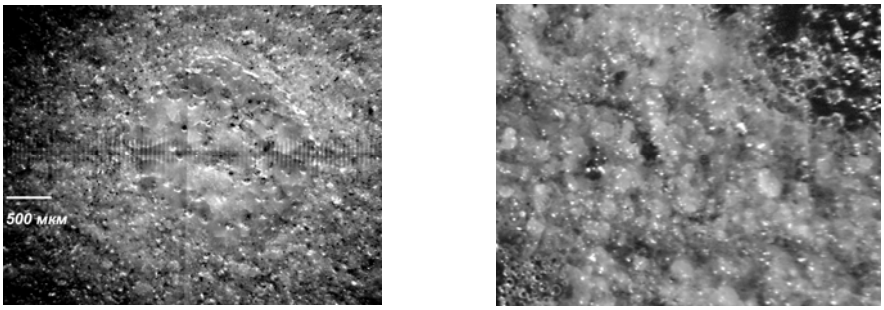

a) b)

Fig. 1. a) Melting spot with pores, q=3.2×10^4 W/cm^2;
b) burn in a thin layer of the coating, q=4.2×10^4 W/cm^2

Laser treatment at certain power densities can lead to a change of nanorelief. When q=3.2×10^4 W/cm^2 laser radiation causes recrystallization and leads to an increase of crystalline grains and their allocation on the surface. Statistical analysis of particle size on the surface shows an increase in the average particle size of 7.34 nm before to 10.52 nm after laser treatment (Fig. 2, 3).

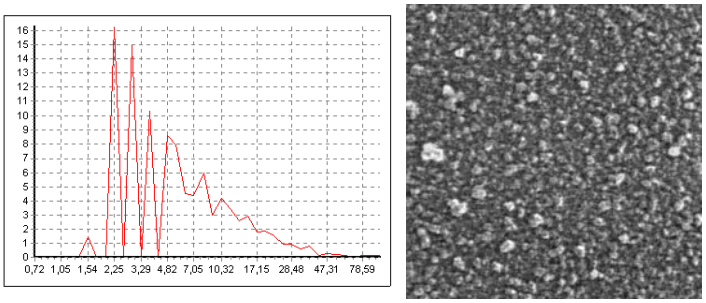

Fig. 2. Size distribution of particles from 2x2 μm surface before laser treatment

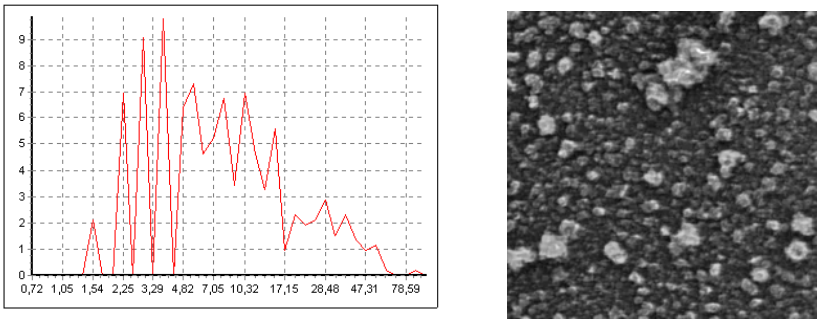

Fig. 3. Size distribution of particles from 2x2 μm surface after laser treatment

Recrystallization is confirmed by X-ray analysis. Initially, there is a large amount of disordered crystallites in the sprayed coating. The growth of the reflections amplitude (Fig. 4) indicates the ordering of the structure and the stabilization of the coating characteristics: increased strength, improved surface properties.

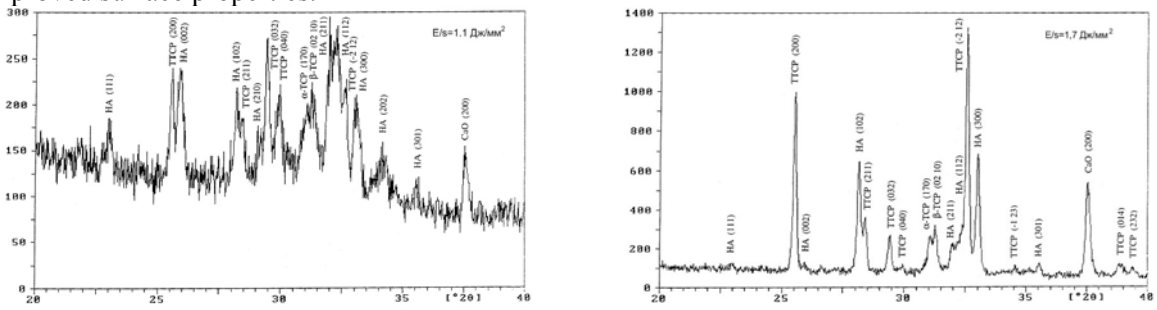

a) b)

Fig. 4. Diffraction pictures of plasma-sprayed coating after laser treatment with a) q=3.2×10^4 W/cm^2 b) 6×10^4 W/cm^2

The HA/TCP phase ratio shows that the coating in Fig. 4a is better than the coating in Fig. 4b. The power density 3.2×10^4 W/cm^2 leads to melting of the surface and a slight increase of the crystalline phase (Fig. 1a). It is important to note that the coating remains porous because of the release of gas bubbles from the structure. Figure 4b shows the high intensity of TCP (2 0 0) and (2 1 2) diffraction; the amount of crystalline phase by 10-15% larger than in Fig. 4a. This is possible due to the higher amount of phase TCP. Increased power density up to 6×10^4 W/cm^2 probably causes the transformation of the amorphous phase to the TCP through recrystallization. Also decrease of phase α-TCP and β-TCP was observed in the coatings without modification phase of calcium oxide [5].

Conclusion. The experiments showed that using a laser to modify the plasma-sprayed coatings under specific modes is an effective method. Laser treatment at power density 3.2×10^4 W/cm^2 causes recrystallization of coating. This slightly increases the content of the crystalline phase (from 24% to 28%). Higher values of power density up to 6×10^4 W/cm^2 provides an increase of the content of the crystalline phase (36%) with the transformation of the amorphous phase to the TCP. As a result, the crystalline grains increase. At this stage, we plan to study mechanical strength of coatings after laser treatment.

Acknowledgements. The work is supported by grant NK-566P/8(5) within the framework of FTP "Scientific and Pedagogical Staff of Innovational Russia" 2009–2013.

References

1. L.M. Sorokin, V.I. Sokolov, A.P. Burtsev, A.V. Kalmykov, L.V. Grigoriev, *Tech. Phys. Letters,* 2007, **33**(24), 69-75.
2. O.V. Dyachenko, *Engineering Phys. Journal,* 2003, **76**(6), 188-191.
3. G.D. Gureev, D.M. Gureev, *Bulletin of Samara STU: Phys.-Math. Sci. Series*, 2007, **2**, 138-144.
4. K.G. Butovskiy, A.V. Lyasnikova, A.V. Lepilin, R.V. Penkin, V.N. Lyasnikov, *Electro-plasma deposition in the manufacture of intraosseous implants*, SSTU Publ., Saratov, 2006, p.200.
5. P. Cheang, K.A. Khor, L.L. Teoh, *Biomaterials*, 1996, **17**, 1901-1904.

Invited

OVERVIEW OF DEVELOPMENTS TOWARDS LASER-PLASMA ACCELERATION BASED X-RAY SOURCES FOR BIOMEDICINE AND OTHER APPLICATIONS IN THE JOHN ADAMS INSTITUTE FOR ACCELERATOR SCIENCE

A.A. Seryi

John Adams Institute for Accelerator Science, University of Oxford and Royal Holloway University of London
United Kingdom, andrei.seryi@adams-institute.ac.uk

Laser-driven accelerators are of enormous current interest not only because they can generate acceleration gradients several orders of magnitude greater than is possible with conventional technology, but also because the beams they produce have unique properties, such as short bunch duration and high brightness.

Rapid progress has been achieved in this area in recent years, including: the generation of quasi-monoenergetic electron beams; reaching the milestone of GeV electron beams; and demonstration of the use of plasma accelerators to drive soft x-ray light sources.

One of the areas with greatest near-term potential is the development of compact laser-wakefield-driven next-generation light sources.

State-of-the-art light sources based on high brightness linacs or synchrotrons have had – and will continue to have – a profound impact in many scientific and technological areas. However, their high cost and large size are barriers to widespread access. Wakefield-driven electron sources would not only bring advantages in terms of smaller scale and reduced cost, but also generate ultrafast electron and photon bunches with synchronization of electrons, visible photons and x-rays at the femtosecond level. This should lead to widespread adoption of these sources.

One of the most appealing applications of laser wakefield accelerators is in the construction of ultra compact light sources. Radiation can be generated by LWFAs by three main approaches. The simplest is based on the so called betatron radiation generated by the electron bunch while it propagates within the laser wakefield. As it does so, the electron bunch undergoes transverse oscillations and produces synchrotron radiation. Radiation at hard x-ray wavelengths has already been detected.

Further research in this field is required to provide a better control of the mechanism of radiation generation and to improve the stability and reliability of the radiation source. The potential of this source in terms of peak brightness is comparable to that provided by third generation light sources.

A second approach is to generate synchrotron radiation by passing the electron beam through an undulator. This technique has already been used to produce radiation at visible and soft x-ray wavelengths. LWFAs have proven their capabilities in generating GeV electron beams with normalized emittance below 1μm, high peak current (tens of kA) in ultra-short pulses (tens of fs) with a modest relative energy spread of 1% or less. These results open the possibility of using the high brightness beams produced by LWFAs for generating radiation at shorter wavelengths.

The John Adams Institute, in collaboration with UK and international partners, is developing the laser-plasma accelerator based X-ray sources, and is also investigating the most suitable applications for first such sources for biomedicine and other fields. An overview of these activities will be given in the presentation.

Acknowledgements

The research described in the presentation is supported by the UK Research Councils STFC and EPSRC, the Royal Society, and the Leverhulme Trust.

References

1. S. Kneip et al., *Nat. Phys*., 2010, **6**, 980.
2. W.P. Leemans et al., *Nat. Phys*., 2006, **2**, 696.
3. T. Robinson et al., *J. Opt. Soc. Am*., 2010, B**27**, 763.

COMPARATIVE STUDY OF HARD TOOTH TISSUES ABLATION BY RADIATION OF YAG: Er AND YLF: Er LASERS

A.V. Belikov, A.V. Skrypnik, and **K.V. Shatilova**

Saint-Petersburg state university of information technologies, mechanics and optics, Saint-Petersburg, Russia
meddv@grv.ifmo.ru, alesch_skrypnik@mail.ru, kshatilova@mail.ru

Introduction

Modern laser technologies have been successfully used in medicine and in dentistry. Erbium lasers are considered to be promising sources for the treatment of dental hard tissues [1]. Erbium lasers radiation used in preventive dentistry due to a number of advantages of the laser method of removing tooth enamel and dentin in comparison with conventional mechanical tools. These advantages include the absence of a smear layer on the cavity walls formed by laser radiation, which leads to better adhesion of filling materials; laser surgery is more comfortable for the patient due to the lack of vibration and pain [1, 2].

Previous investigations [3] show that the texturing of the hard tissues surface by a single-mode YAG: Er laser stimulates the increase in the adhesion of some modern light-cured materials to hard tooth tissues. Pulse energy of YAG: Er laser was ~1 mJ, pulse duration was ~100 μs, pulse repetition rate was 1 Hz. Regular sequence of single laser microcraters (texture) was created by laser radiation on hard tissue surface. The diameter of microcraters (texture elements) was ~100 μm, depth was ~ 45 μm.

Currently, new laser sources for the effective implementation of such operations are searched. Diode-pumped YLF: Er laser can become one of such sources; it allows obtaining lasing at different wavelengths: 2.66 μm and 2.81 μm [4]. Diode pumping leads to a significant reduction in weight and size characteristics of the dental laser. This is a significant advantage over the modern lamp-pumped lasers.

Materials and methods

We used YAG: Er (λ = 2.94 μm) and YLF: Er laser (λ=2.66 μm) with pulse duration (base line) of ~130 μs and YLF: Er laser (λ=2.81 μm) with pulse duration (base line) of ~1400 μs in free-running mode. Enamel or dentin surface was polished with a diamond disk before laser irradiation. Laser treatment of dental tissue was carried out in non-contact mode. Laser radiation was focused on the surface with a collecting lens. Flat surface area was exposed by single laser pulse. The energy of a single laser pulse was ~1 and 2 mJ; the energy density was ~9 J/cm^2 and ~19 J/cm^2. Samples were photographed after laser treatment and then it was sawed along the microcrater axis and photographed again. According to received photographs we measured the geometric parameters of microcraters (diameter D, depth h), the volume of microcrater V and removal efficiency $<Eff>$ of tissue were calculated. Removal efficiency of tissue was the ratio of microcrater volume to the energy expended in its formation.

Textures were created on the surface of the enamel and dentin with the distance between the microcraters centers of 100 μm. Each texture was consisted of 100 elements (microcraters) and covers an area approximately 1 mm^2.

Results

YLF: Er laser pulse energy of 1 mJ was not enough for enamel destruction, so we carried out further comparisons for YLF: Er laser pulses with an energy of 2 mJ and YAG: Er laser pulses with an energy of 1 mJ.

During the formation of microcraters by YAG: Er laser radiation in enamel: D=99±3 μm, h=45±8 μm, V=(24±8)×10^{-5} mm^3, $<Eff>$=240±80 mm^3/kJ; in dentine: D=101±1 μm, h=46±4 μm, V=(27±7)×10^{-5} mm^3, $<Eff>$=266±61 mm^3/kJ. During the formation of microcraters by YLF: Er laser radiation (λ=2.66 μm) in enamel: D=105±4 μm, h=42±4 μm, V=(23±5)×10^{-5} mm^3, $<Eff>$=118±20 mm^3/kJ; in dentine: D=118±2 μm, h=49±4 μm, V=(30±7)×10^{-5} mm^3, $<Eff>$=155±26 mm^3/kJ. During the formation of microcraters by YLF: Er laser radiation (λ=2.81 мкм) in enamel: D=115±7 μm, h=32±4 μm, V=(16±6)×10^{-5} mm^3, $<Eff>$=82±20 mm^3/kJ; in dentine: D=155±5 μm, h=26±2 μm, V=(19±4)×10^{-5} mm^3, $<Eff>$=100±21 mm^3/kJ.

Photo of texture formed by the YLF: Er diode-pumped laser radiation (wavelength of 2.81 μm, single pulse, pulse energy of ~2 mJ, energy density of ~19 J/cm^2, pulse duration of ~1400 μs) is shown in Fig. 1. Photographs were obtained with a light microscope AxioScope A1 and a digital camera AxioCam (Carl Zeiss) in reflected light (dark-field microscopy).

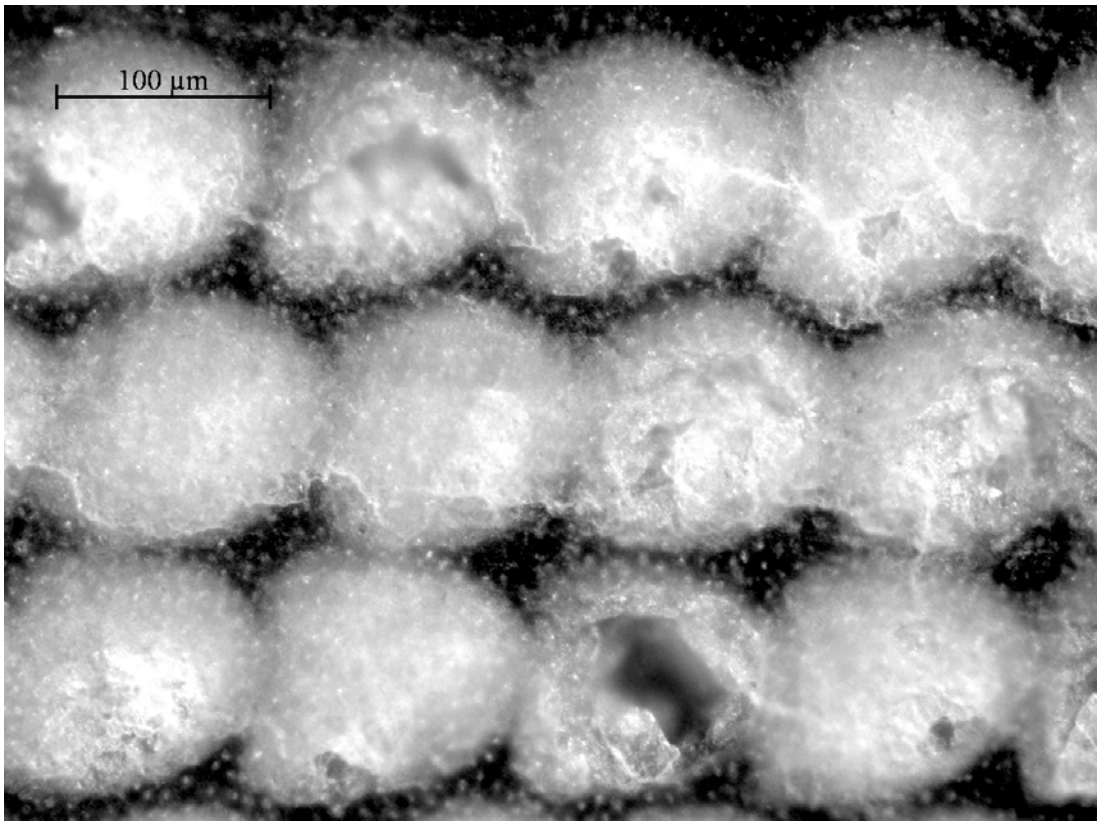

Fig. 1. Typical photo of texture formed by the YLF: Er diode-pumped laser radiation with 2.81 μm wavelength

Conclusions

Interaction of YAG: Er (wavelength is 2.94 μm) and YLF: Er (wavelengths are 2.66 μm or 2.81 μm) lasers radiation with hard tooth tissues were investigated. The diameter, depth and volume of the craters, enamel and dentin removal efficiency by erbium lasers radiation were determined. Textures were created on the surface of the enamel and dentin with the distance between the microcraters centers of 100 μm by YAG: Er and YLF: Er lasers radiation. Mechanisms of ablation and comparing removal efficiency of hard tooth tissues by different Er lasers radiation were discussed.

References

1. D.J. Coluzzi and R.A. Convissar, *Atlas of laser applications in dentistry*. Quintessence book, 2007, p 220.
2. H.-P. Berlien and G.J. Müller, *Applied Laser Medicine,* Springer-Verlag, Berlin, Heidelberg, New York, 2003, p. 740.
3. A.V. Belikov, A.E. Pushkareva, A.V Skrypnik, T.V. Strunina, and K.V. Shatilova. *News of high schools. Instrument-making*, 2010, **53**(4), 52-56.
4. M.V. Inochkin, V.V. Nzarov, D.U. Sachkov, L.V. Khloponin, V.U. Khramov. *Journal of Optical Technology*, 2010, **77**(7), 8-13.

Invited

UPGRADE OF PETAWATT-LEVEL PEARL LASER FOR MEDICAL APPLICATIONS

A.A. Shaykin, V.N.Ginzburg, E.V. Katin, E.A. Khazanov, V.V. Lozhkarev, G.A. Luchinin, A.N. Mal'shakov, M.A. Martyanov, A.K. Poteomkin, A.A. Soloviev, and **I.V. Yakovlev**

Institute of Applied Physics RAS, Nizhny Novgorod, Russia, shaykin@appl.sci-nnov.ru

A unique 0.56 PW laser PEARL was created at IAP RAS in 2007 and in 2009 the first experiments on electron acceleration were carried out. A powerful (about 10^{20}W/cm^2) laser is broadly used in basic studies of the mechanisms of the laser-matter interaction. Applications include but are not restricted to development of compact electron beam accelerators [1] for linear accelerators or free electron lasers; creation of a multicascade optical accelerator of electron bunches; development on new sources of X-ray and gamma radiation [2] for dense plasma diagnostics; attosecond pulse generation for diagnostics of fast processes in neuclei and atoms; creation of compact proton and light ion accelerators for protonography and hadron therapy of tumors; generating proton beams for nuclear fusion facilities with fast ignition [3]. Each application demands a laser with specific properties. High pulse repetition rate and a flexible system controlling radiation parameters are needed for the great majority of laser applications. Currently, several multipetawatt power systems are developed. These include Vulcan-10PW (The Rutherford Laboratory in England), ILE_Apollon (The PanEuropean project in the framework of ELI). The merits of the multipetawatt level created in our institute as compared to the other systems are its compact size and simple scaling. A few interesting physical problems have been solved during its development, which will enable us to create a unique laser.

The laser is installed in a 300 m^2 basement, where a clean room, a control room, a target chamber, and a vacuum system are available. The area of the clean room is 180 m^2.

The laser is a three-cascade DKDP crystal parametric amplifier. A Cr:Fr femtosecond generator with pulse duration of 40 fs and energy of 5 nJ is used as a master oscillator. The pulse is stretched up to the duration of 0.6 ns and is transmitted to the first parametric amplification cascade. Two optical pulses: at 1250 nm and 910 nm are available at the crystal output, with energies of 90 and 110 μJ, respectively. As DKDP crystals have superbroadband stynchronism near 910 nm, we use a 910 nm pulse in the second and third cascades of parametric amplification. The second harmonic of Nd:YLF laser having duration 1 ns and energy over 1 J pumps the first two cascades of the parametric amplifier. We synchronize signal and pump pulses with jitter less than 40 ps [4]. This allows obtaining stable parameters of output optical pulse: energy of 100 mJ, central wavelength 910 nm, spectrum not less than 40 nm. For pumping the terminal parametric amplification cascade the second harmonic of Nd:glass laser is used with pulse duration of 0.9 ns, energy about 200 J, and duty factor more than 0.8. Two pump lasers are synchronized by means of an optical delay line allowing precision adgustment for compensating the delay associated with distortion of pulse shape in the glass amplifier. This provides a signal up to 24 J. Further the pulse is compressed in a four-grid compressor located in the vacuum chamber. The PEARL laser has the following parameters of output radiation: duration 43 fs and energy 24 J. The use of parametric amplification allows attaining high contrast. It was about 10^4 in the ps windowband about 10^8 beyond 10-15 ps [5]. Albeit our laser has no record values of some parameters (there exist systems with shorter pulse duration or higher energy, or higher pulse repetition rate), the combination of its features makes it a unique optical system [6].

The use in the pump laser of quantrons of novel design will enable the pulse repetition rate to be reduced from 35–40 min to 3–5 min. For enhancing optical pulse energy we changed the Nd:glass laser scheme. Pump energy will be increased up to 300 J. Pulse shape (temporal) will be closer to a stepwise. This will permit spreading the spectrum of the amplified chirped pulse and reducing pulse duration after compression down to 30-35 fs. The energy of the amplified pulse will be about 50 J. Contrast may be enhanced due to generation of the second harmonic of fs pulse. Spectrum spreading at second harmonic generation may be used for additional fs pulse shortening down to 12 – 18 fs [7].

In the near future we are planning to install one more parametric amplification cascade with pumping of 600 J. Thus, the output pulse power may be increased up to 5 PW. We expect that this will allow generating proton beams with energies of 200-300 MeV and energy spread of several percent that are demanded for medical applications.

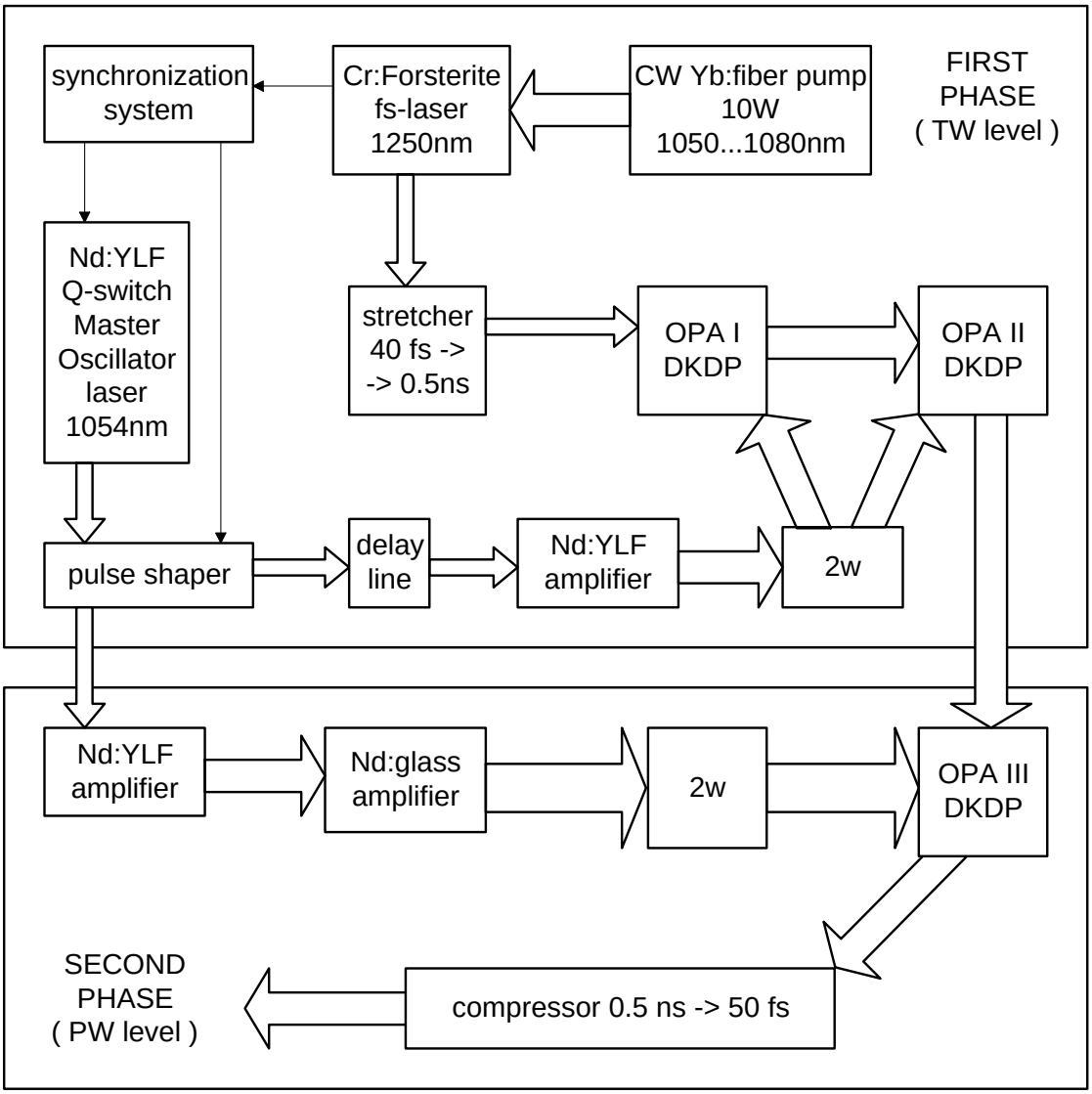

References

1. E. Esarey, C.B. Schroeder, W.P. Lemans, *Rev.Mod. Phys.,* 2009, **81**(3), 1229-1285.
2. U. Teuber, P. Gibbon, *Rev.Mod.Phys.,* 2009, **81**(2), 45-79.
3. M. Tabak, D.S. Clark, S.P. Hatchett, M.H. Key, B.F. Lasinski, R.A. Snavely, S.C. Wilks, R.P.J. Town, R. Stephens, *Physics of Plasmas,* 2005, **12**(5), 057305.
4. G. Freidman, N. Andreev, V. Ginzburg, E. Katin, E. Khazanov, V. Lozhkarev, O. Palashov, A. Sergeev, I. Yakovlev, *Proc. SPIE,* 2002, **4630**, 135-146.
5. V.N. Ginzburg, N.V. Didenko, A.V. Konyashchenko, V.V. Lozhkarev, G.A. Luchinin,G.A. Lutsenko, S.Yu. Mironov, E.A. Khazanov, I.V. Yakovlev, *Quantum Electronics*, 2008, **38**(11), 1027-1032.
6. V. Lozhkarev, G. Freidman, V. Ginzburg, E. Katin, E. Khazanov, A. Kirsanov, G. Luchinin, A. Mal'shakov, M. Martyanov, O. Palashov, A. Poteomkin, A. Sergeev, A. Shaykin, I. Yakovlev, *Laser Physics Letters,* 2007, **4**, 421-427.
7. S.Y. Mironov, V.V. Lozhkarev, V.N. Ginzburg, E.A. Khazanov, *Applied Optics,* 2009, **48**(11), 2051-2057.

PROSPECTS OF PEARL MEDICINE

A.A. Soloviev

Institute of Applied Physics, Russian Academy of Sciences
46 Ulyanov st., Nizhny Novgorod 603950, Russia
so_lo@appl.sci-nnov.ru

From the medical point of view, the PW-class laser systems including the PEARL laser facility [1] (PEtawatt pARametric Laser, IAP RAS, Nizhny Novgorod, Russia) are most interesting thanks to the possibility of creating very effective and compact secondary radiation sources. The focusing of PW laser pulse on a gas or solid target can lead to generation of electron [2], proton [3], or ion beams, X-ray and gamma-quanta, atto- and zeptosecond pulses [4]. The protons can be used in the hadron therapy for cancer treatment [5]. Laser accelerated electrons can be used for short-lived radionuclide generation in positron emission tomography (PET) [6] or can pump a free-electron laser [7] for phase-contrast X-ray imaging of biological tissue or human surgery as well. Attosecond pulses can be used for studying biological molecule dynamics [8]. Moreover, the interesting physics and the whole spectrum of scientific and engineering problems are behind each of the secondary radiation types.

The paper is concerned with prospects of a PEARL based experimental complex creation for carrying out some medical experiments, with different types of ionizing radiation in particular. The power of the laser is sufficient for the applications mentioned above.

An experimental series of LWFA (laser wakefield acceleration) electron beam production conducted at IAP RAS can serve as a good confirmation of the prospects. During the experimental series the experimental-diagnostics equipment was developed and the unique single-shot PW laser utilization experience was acquired. A schematic diagram of the experiments is presented in Fig. 1.

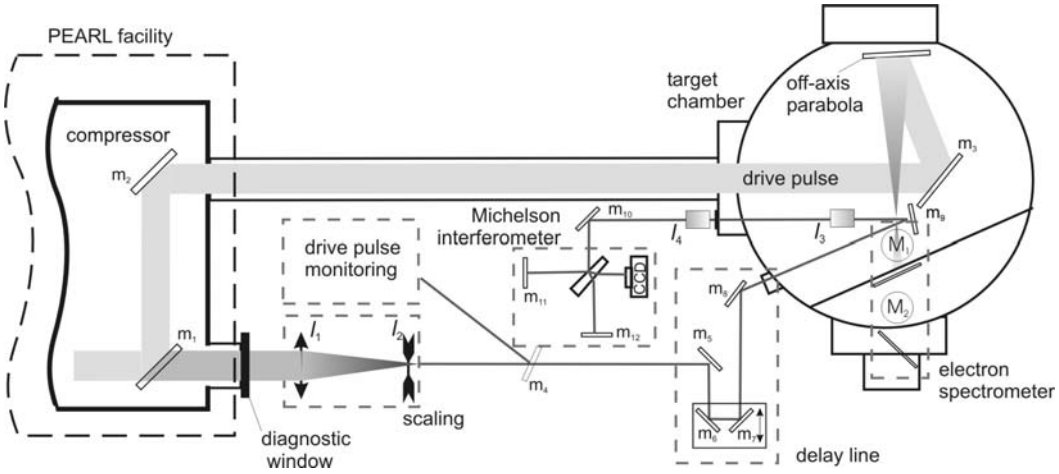

Fig. 1. Experimental LWFA complex at PEARL facility:
m_1–m_{12} are mirrors, l_1–l_4 are lenses, M_1–M_2 are magnets

The main PEARL pulse after compressor is split into two parts. The powerful pulse then serves as a driver coming after the compressor into the target chamber where it is focused into a supersonic gas jet by means of an off-axis parabolic mirror with f/15 or f/6 forming the focal spot sizes of the laser beam of 18 and 7.2 mm at FWHM intensity, respectively. The average laser intensities correspond to the normalized vector potential $a_0 = 2$ and 7, respectively. The second part with a much lower power transmitted by the mirror m1 arrives at the diagnostic channel where it is used for monitoring the driver and for the interferometric diagnostics of plasma density [2].

It should be noted that an original two-screen electron energy spectrometer [9] was utilized in the work. The schematic diagram of the spectrometer is presented in Fig. 2. The use of the single-shot electron spectrometer with two scintillators allows reaching an accuracy of 30 MeV for mean energy and ±10 MeV for the energy spread of 300 MeV beam with 30 MeV energy spread. Such accuracy is obtained for a 40 cm long spectrometer with 0.7 T × 9 cm constant magnet system. The angle of entry into the magnetic system, α, ranges from zero to fractions of radian. The impact of the small-angle

electron scattering in the bulk of the first scintillator was assessed theoretically and measured in experiments. It was shown that spectra of the beams having average energy higher than 200 MeV may be measured to high accuracy if this effect is neglected. A simple method of enhancing accuracy of placing scintillating screens by means of an optical reference point is proposed. The method is based on using a small portion of pump PW laser radiation for taking into consideration mutual transverse displacement of the scintillators. The measurement accuracy greatly exceeds that of a one-screen spectrometer with analogous size and magnetic field.

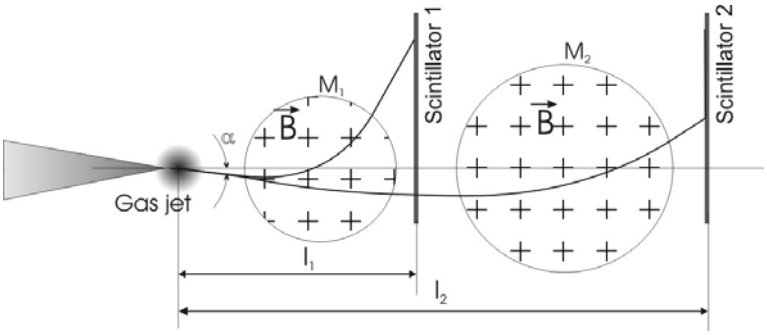

Fig. 2. Schematic of the two-screen electron spectrometer

The LWFA complex has been created on the basis of the PEARL facility that generates, in different shots, quasi-monoenergetic electron beams with energies up to 300MeV, minimum angular size of 6 mrad FWHM, and charge as large as 300 pC [2]. In view of relatively low stability of parameters of laser radiation much attention was focused on measuring parameters of each LWFA.

Conical supersonic gas nozzles producing homogeneous distribution of gas with characteristic size 1, 3, 5, and 8 mm were developed and optically calibrated. Direct interferometric diagnostics of plasma density was done. Electron beams were observed above the threshold $P = 2 \cdot P_c$. Qualitative dependence of the behaviour of the generated beams on plasma density has been considered. For the focusing angle f/15, experiments demonstrated a tendency to electron beam energy increase with decreasing plasma density in the $9 \cdot 10^{18}$– $3 \cdot 10^{18}$ cm^{-3} range. This dependence is in a good agreement with the phenomenological theory described in Ref. [10]. It was demonstrated in experiments that the angular size of the electron beams decreases with the increase of their mean energy for helium and nitrogen jets 5 and 10 mm in diameter.

The conducted experiments are promising for successful implementation of the secondary radiation complex on the base of PEARL laser, including a wide spectrum of medical studies.

Acknowledgements

This research was supported by the Presidium of RAS, the RFBR (Grants No. 09-02-12322-ofi_m, No. 11-02-97095-r, and No. 11-02-01070-a), the Presidential Council on Grants of the Russian Federation (Grant No.3800.2010.2) and the Ministry of Education and Science of the Russian Federation (contract No. 02.740.11.0225).

References

1. V. Lozhkarev, et al., *Laser Phys. Lett*., 2007, **4**(6), 421.
2. A.A. Soloviev, et al., *Nucl. Instr. And Meth. A*, 2011, doi:10.1016/j.nima.2011.01.180.
3. B.M. Hegelich, et al., *Nature*, 2006, **439**, 26 January.
4. Y. Nomura et at., *Nature Physics*, 2009, **5**, 124-128.
5. Petti and Lennox, *Hadronic Radiotherapy, Ann. Rev. Nuclear & Particle Science*, 1994, **44**, 154-197.
6. M. Ter-Pogossian, et al., *Radiology*, **114**(1), 89-98.
7. J. Madey, *J. Appl. Phys*., 1971, **42**, 1906.
8. M. Kling, et al., *Annu. Rev. Phys. Chem*., 2008, **59**, 463-92.
9. A. Soloviev, et. al., *Rev. Sci. Instrum*., 2011, **82**, 043304.
10. W. Lu, et al., *Phys. Rev. Spec. Top. Acceler. Beams*, 2007, **10**, 061301.